Clemson University
TigerPrints

All Theses Theses

8-2011

Risks Posed to Drinking Water Aquifers Due to Leakage of Dissolved CO2 in Improperly Abandoned Wellbores

Kirk Ellison
Clemson University, kirke@g.clemson.edu

Follow this and additional works at: http://tigerprints.clemson.edu/all_theses

Part of the Geology Commons

Recommended Citation
Ellison, Kirk, "Risks Posed to Drinking Water Aquifers Due to Leakage of Dissolved CO2 in Improperly Abandoned Wellbores" (2011). *All Theses.* Paper 1177.

This Thesis is brought to you for free and open access by the Theses at TigerPrints. It has been accepted for inclusion in All Theses by an authorized administrator of TigerPrints. For more information, please contact awesole@clemson.edu.

RISKS POSED TO DRINKING WATER AQUIFERS DUE TO LEAKAGE OF DISSOLVED CO_2 IN IMPROPERLY ABANDONED WELLBORES

A Thesis
Presented to
The Graduate School of
Clemson University

In Partial Fulfillment
Of the Requirements for the Degree
Master of Science
Environmental Engineering and Earth Sciences

---

by
Kirk Matthew Ellison
August 2011

Accepted by:
Dr. Ronald Falta, Committee Chair
Dr. Lawrence Murdoch
Mr. Scott Brame

ABSTRACT

In order to ensure safe long-term storage of carbon dioxide in geologic formations, the risks posed by improperly abandoned wells must be understood and minimalized. In addition to supercritical and gaseous CO_2, brine containing dissolved CO_2 poses a leakage risk. CO_2 dissolution in brine leads to denser brine and better long-term storage security, but its leakage risk is not zero. Under specific circumstances with formation overpressure or overlying aquifer drawdown, dissolved brine can flow up improperly abandoned wells where it can potentially enter and contaminate drinking water aquifers. The possibility that depressurization in the wellbore may cause CO_2 exsolution from brine to form a separate buoyant gas phase is of primary concern. Analytical as well as numerical models are used to evaluate these effects in wellbores as well as to examine the effects of system parameters on brine leakage rates through wellbores.

A simple analytical model for uniform density flow is used to evaluate the effects of physical parameters on fluid leakage. It is a useful screening tool for estimating leading order effects of system parameters on leakage of CO_2 laden brine. The TOUGH2-ECO2N simulator is also used to evaluate wellbore leakage of dissolved CO_2 considering gas exsolution due to pressure, temperature, phase, and salinity changes.

Simulations identify the conditions under which a separate gas phase exsolves in a wellbore during CO_2 laden brine leakage. Up to 20% of the dissolved brine is found to exsolve in the numerical simulations. This gas accumulates along the top of a drinking water aquifer as a buoyant phase. Simulations also show that the degree of leakage is constrained by the properties of the well, with the permeability of the well being of chief

importance. However, at high well permeabilities, simulations show that the geologic formations provide more resistance to flow than the well and constrain leakage rates. Additional analyses are performed in order to see how dissolved CO_2 may leak from a wellbore in a geologic system of stratified permeable layers. It is found that the presence of stratigraphy limits the possibility of upward migration of dissolved CO_2, whether through overpressure of drawdown.

Table of Contents

Page

ABSTRACT ii

LIST OF FIGURES vi

LIST OF TABLES ix

1. INTRODUCTION 1

2. APPROACH 7

3. BASE CASE MODELS 7

3.1 Analytical Model 7

3.1.2 Dimensionless Analysis 13

3.2 Base Case Numerical Model 17

3.3 Comparison of Analytical and Numerical Models 22

3.4 Flow Effects Due to Changing Well Permeability 26

3.5 Flow Effects Due to Changing Wellbore Diameter 35

3.6 Flow Effects Due to Salinity 37

3.7 Flow Effects Due to Various Overpressures and Drawdowns 40

3.7.1 Overpressure Effects 40

3.7.2 Drawdown Effects 42

3.8 Leakage Plume Behavior Post Injection 46

3.9 Comparing Supercritical CO_2 Leakage to CO_2 Dissolved Brine Leakage 48

4. SIMPLE STRATIFIED MODEL 51

4.1 Overpressure 52

Page
4.2 Effects of DWA Drawdown 55

4.3 Dissolved CO_2 Injection into Interbedded Formations
Connected by an Open Well 57

5. WABAMUN LAKE STRATIFIED MODEL 59

5.1 Leakage from Basal Cambrian Formation 63

5.2 Leakage from Wabamun Lake Formation 64

6. SUMMARY 66

APPENDIX A 68

7. REFERENCES 70

LIST OF FIGURES

Figure Page

Figure 1: Dependence of aqueous solubility of CO_2 on pressure and temperature at a salinity of 2% by mass. 6

Figure 2: Conceptual Drawing of the analytical model's geometry and parameters. a) Conceptual models with arrows indicating the direction of flow. b) Drawing showing the variables used in the analytical model. 8

Figure 3: Dimensionless flow rate for the model showing at what well conductances the overall flow rate is controlled by the geologic media or the wellbore. 17

Figure 4: Base case numerical model setup. The storage formation and DWA are separated by a 1000-meter thick impermeable layer. All formations are penetrated by a well in the central radial element. 18

Figure 5: Comparison of the laminar and turbulent flow analytical solutions for a range of well permeabilities. Laminar flow in the wellbore under Darcy's law from equation 10 converges to the turbulent Darcy-Weisbach pipe flow from equation 13 at well permeabilities higher than $1x10^{-6}$ m^2 for parameters used in subsequent numerical simulations. 25

Figure 6: Changing solubility of CO_2 in the wellbore with changes in pressure and temperature. For parameters from the numerical model, initial static conditions suggest exsolution will not occur until 60 bar (-600 m) is crossed by the leaking brine. Increasing pressure allows the con to stay in solution until 50 bar (-500 m). Over time, thermal effects increase temperature in the wellbore. This decreases solubility along the wellbore such that exsolution occurs at 100 bar (-1000 m) 28

Figure 7: Dissolved and gaseous CO_2 plume in the drinking water aquifer at various well permeabilities at 50 years. Well permeabilities are not shown where plume formation is not significant. 30

Figure 8: Total CO_2 flow rate into the DWA at various well permeabilities. 31

Figure 9: Steady-state aqueous flow rate at various well permeabilities for both the numerical and analytical models. 33

Figure 10: Simulation results showing the simulated mass of CO_2 leakage plumes in the DWA as a function of well permeability and formation overpressure..... 34

Figure 11: Numerical and analytical aqueous flow rates as a function of changing well radius at several wellbore permeabilities..... 37

Figure 12: Brine flow rate into the DWA at various salinities with and without dissolved CO2..... 39

Figure 13: Brine flow rate into the DWA at various overpressures and drawdowns. 45

Figure 14: Exsolved gaseous CO_2 flow rate into the DWA at various overpressures and drawdowns..... 45

Figure 15: Dissolved CO_2 plume migration in the entire system and in the DWA after 100 years of leakage due to overpressure. 46

Figure 16: Dissolved CO_2 plumes in the DWA at 50 years for both supercritical and CO_2 laden brine leakage models. 51

Figure 17: Gaseous CO_2 plumes in the DWA at 50 years for both supercritical and CO_2 laden brine leakage models. 51

Figure 18: Dissolved and gaseous leakage plumes at 50 years for the stratified simulation at 50 years of leakage..... 53

Figure 19: Dissolved and gaseous leakage plumes at 50 years for the 150,000 mg/l salinity stratified simulation at 50 years of leakage. 55

Figure 20: Horizontal brine flow rate along the wellbore due to DWA drawdown at 50 years in the stratified simulation..... 56

Figure 21: Vertical brine flow rate along the wellbore due to DWA drawdown at 50 years in the stratified simulation. 56

Figure 22: Dissolved and gaseous CO_2 plumes due to leakage from a stratified layer at 50 years. 59

Figure 23: Model setup for Wabamun Lake stratified model showing the three rock types used and the 37 model layers. 60

Figure 24: Dissolved leakage plume due to injection into the Basal Cambrian formation at 50 years (note that the top depth is only -1800 m). 64

Figure 25: Dissolved leakage plume due to dissolved CO_2 leakage from the Wabamun formation at 50 years (note that the top depth is only -1600 m). 65

LIST OF TABLES

Table Page

Table 1: Analytical and Numerical Model Parameters 12

Table 2: Material Properties for Analytical and Numerical Models 13

Table 3: Relative Permeability and Capillary Pressure Parameters for Base Case Model 22

Table 4: Model Validation Showing Well Permeability vs. Flow Rate 24

Table 5: Model Validation of Overpressure vs. Flow Rate 26

Table 6: Gas Phase Fraction in DWA Compared to Equilibrium Values 29

Table 7: Numerical Flow Rates Due to Overpressure 42

Table 8: Rock Properties for Wabamun Lake Stratified Model 61

Table 9: Relative Permeability and Capillary Pressure Parameters for Wabamun Lake Stratified Model 62

1. **INTRODUCTION**

Mitigation of increasing levels of CO_2 will require a multitude of different strategies. Due to the tremendous amounts of CO_2 being emitted, geologic carbon sequestration is gaining traction as a viable and scientifically feasible way to reduce greenhouse gas emissions. In 2009, the United States total emissions of greenhouse gases were 6,633.2 million metric tons of CO2 equivalents (EPA, 2011). NETL (2010), estimates a CO_2 storage capacity for the United States and Canada of 1,850 to 20,470 billion metric tons in geologic formations, representing at least 450 years of storage capacity.

In order to gain public trust, a complete understanding of potential risks due to CCS as well as a suite of viable mitigation strategies needs to be established. With respect to risk, the possibility of CO_2 leakage from storage formations is considered the most likely and widespread threat to storage security. Currently, the goal is that 99% of injected CO_2 will remain sequestered over a period of 1,000 years (IPCC, 2005). Therefore, an adequate understanding of all foreseeable leakage scenarios needs to be gained.

Current EPA regulations for CO_2 injection under the Underground Injection Control program require definition of an area of review for injection. For CO_2 injections, the boundary of this area is likely to be defined as the radial extent of the pressure front induced due to injection. Within the area of review, the EPA requires identification, monitoring, and if necessary, mitigation of all leakage pathways that intersect the storage formation or its sealing unit.

Considering all probable leakage pathways, abandoned wells are thought to pose one of the highest risks (Gasda et al., 2004; IPCC, 2005; Nicot, 2009; Nordbotten et al., 2005;

Pruess, 2008). In the United States, oil and gas wells have been drilled for nearly 150 years. This has led to hundreds of thousands of wells that penetrate the subsurface (Gasda et al., 2004). Of all these wells, it is believed that improperly abandoned or degraded wellbores pose the most serious threat (IPCC, 2005).

Since 1952, wells cements have had the appropriate additives to create a proper plug (Ide et al., 2006). In addition, by the 1950's most states put in place sufficient well abandonment regulations. However, prior to this, well abandonment procedures were questionable. Before the 1950's it is uncertain whether cement plugs were even effective. Early cements lacked sufficient additives for proper hardening at down-hole pressures and temperatures. In fact, such primitive techniques as pouring ice down the well to lower borehole temperature were used to try to achieve proper cementation. Furthermore, it is documented that many of the cement plugs from the Gulf Coast before the 1930's were contaminated with drilling mud (Smith, 1976).

In the early stages of oil and gas drilling, it is likely that many boreholes were abandoned without ever being effectively plugged. When early wells were plugged, they were often filled with materials that were readily available. Well plugs discovered from the early 1900's have been found to contain materials such as logs, mud, and animal carcasses (Ide et al., 2006).

Many of these early wells are poorly sealed. However, many of them are only drilled to relatively shallow depths. Therefore, they may not pose a direct leakage risk to sequestration formations. However, leakage from a secondary CO_2 plume is a still a relevant concern. In addition, some of these early wells do penetrate formations at a

depth feasible for carbon sequestration (Gass et al., 1977). In addition to leaking through these unsealed wells, it is possible that injected CO_2 could degrade the integrity of properly sealed wellbores. Such leakage pathways include leakage through the cement, through corroded casing, and through the well annulus (Gasda et al., 2004).

Currently there are few data on the physical properties of abandoned wells. To date much research has been focused on how supercritical or gaseous CO_2 may leak up wellbores (Ebigbo et al., 2007; Ide et al., 2006; Nordbotten et al., 2005; Nordbotten et al., 2009; Pan et al., 2009). Other work has focused on potential aquifer contamination due to upward migration of brine through abandoned wellbores (Nicot, 2009; Birkholzer et al., 2011).

While gaseous leakage up a poorly sealed wellbore likely represents the highest risk from abandoned wells, other mechanisms exist whereby CO_2 could leak upward. Wellbore leakage of dissolved phase CO_2 is a possible scenario that has only been studied by a few researchers (Pruess, 2008; Pan et al., 2009).

It is expected that injected supercritical CO_2 will eventually dissolve into the storage formation brines over time-scales of hundreds to thousands of years (McPherson and Cole, 2000; Ennis-King and Paterson, 2003). Moreover, some researchers have proposed injecting CO_2 as a dissolved phase (Burton and Bryant, 2007; Leonenko and Keith, 2008; Burton and Bryant, 2009). Once CO_2 is dissolved into storage formation brines, a buoyant gaseous CO_2 phase no longer exists. Upon dissolution the brine becomes about 1% denser (Enick and Klara, 1990; Bachu and Adams, 2003), therefore it will have a tendency to sink slowly to the bottom of the formation.

While it is less likely that dissolved CO_2 will leak up abandoned wellbores, there is still a potential danger. If the storage formation is overpressured, or if an overlying aquifer is drawn down due to pumping, the pressure differential could induce the brine containing the dissolved CO_2 to flow upward through permeable pathways such as abandoned wells. In addition to CO_2 laden brine contaminations of overlying aquifers and potential drinking water sources, as it rises the CO_2 has the potential to exsolve and form a separate gas phase. Due to a decrease in pressure as the leaked brine moves upward, CO_2 solubility decreases causing gas phase exsolution (Pruess, 2008). This gas phase then has the potential to accumulate in drinking water aquifers or potentially migrate to the surface due to its buoyancy.

Previous studies concerning brine leakage through wellbores has shown that in order for prolonged brine leakage to occur, a pressure threshold must be crossed, and sustained. For brine leakage, research has focused on leakage near area of review boundaries, where formation overpressures due to injection may be low (Birkholzer et al., 2011; Nicot, 2009). Zhou et al. (2010) showed that overpressures as high as 35 bar may be typical for commercial scale CO_2 injection. In scenarios where dissolved brine exists only due to equilibration with resident brine over time, it is expected that significant residual overpressure will remain many years after injection has ceased (Zhou et al., 2010). If CO_2 is injected as a dissolved phase, resulting overpressures will be at least as high as expected overpressures for supercritical injection.

The focus of this thesis is to examine what properties in an abandoned wellbore control the overall flow rate for leakage of brine containing dissolved CO_2. In addition,

gaseous CO_2 exsolution effects and leakage plumes are examined. In Contrast to recent similar studies by Birkholzer et al. (2011), whose focus is brine leakage through wellbores near the area of review boundary, the focus of this research is specifically directed toward wellbore leakage of CO_2 laden brine. Investigation of how this dissolved phase CO_2 could leak up wellbores and contaminate overlying drinking water aquifers (DWA) is of primary concern. Distinctive from other studies, wellbore leakage of dissolved CO_2 laden brine due to not only storage formation overpressure, but also overlying aquifer drawdown are examined.

Birkholzer et al. (2011) examined some brine flow effects due to changes in system parameters such as well permeability and degree of overpressure. In this study, changes in flow due to system parameters are examined in detail. Flow effects when multiple permeable formations are present along the wellbore are also considered. In addition, an analytical model is proposed that can provide insights into leading order flow behavior due to various parameters.

Unique flow effects that occur due to the presence of dissolved CO_2 are also investigated. As the CO_2 laden brine migrates upward, gas exsolution can induce changes in temperature and pressure as well as change effective permeabilities in the system.

Gas exsolution can occur during wellbore leakage due to a decrease in the solubility of CO_2. The solubility of CO_2 is dependent on the pressure, temperature, and salinity of the brine. The solubility of CO_2 over a range of pressure and temperature conditions at a

salinity of 20,000 mg/l, which is representative of low-salinity brine, can be seen in figure 1.

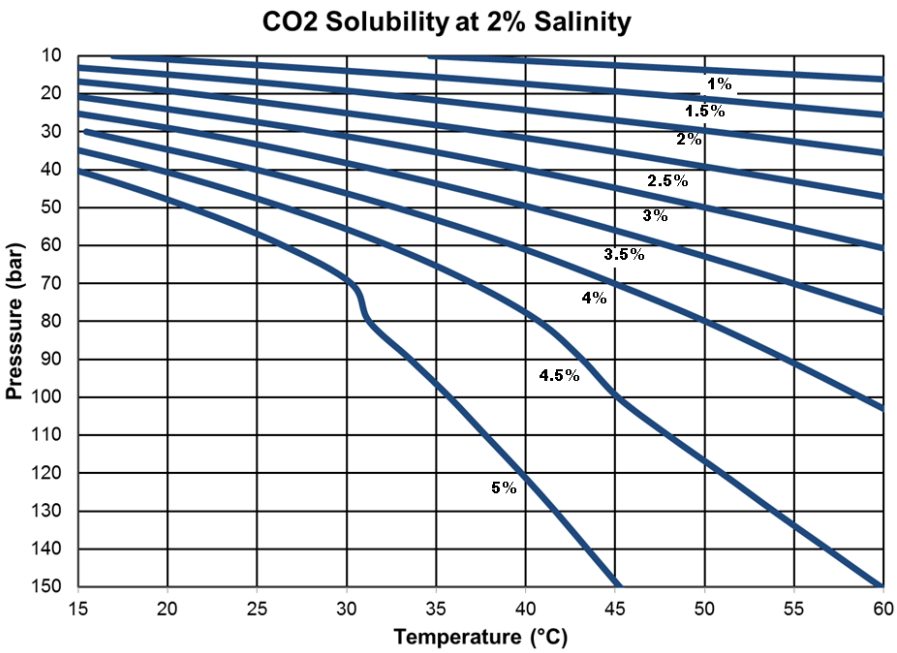

Figure 1: Dependence of aqueous solubility of CO_2 on pressure and temperature at a salinity of 2% by mass.

The solubility of CO_2 at typical storage formation pressures and temperatures (75-150 bar; 30-60°C), is 4-5% by mass for a low salinity brine. However, at shallower depths corresponding to a DWA a few hundred meters below the ground surface, where the pressure and temperature is between 10-30 bar and 15-30°C, CO_2 solubility drops to 2-3% or less. Therefore, if upward migration of CO_2 laden brine occurs, it is possible for 40% or more of the originally dissolved CO_2 to exsolve during upward transport. As a part of this study, the numerically simulated amount of exsolved CO_2 is examined and compared to equilibrium calculations of the expected gas fraction in order to quantify expected risks due to gaseous plume evolution.

Currently there are little data on the physical properties of abandoned wells. For example, leaky wellbore flow properties could potential range over many orders of magnitude from slightly permeable due to fissures and cracks in well cements to a completely open pipe (Birkholzer et al., 2011).

2. APPROACH

To understand and quantify the factors that may control CO_2 laden brine leakage rates into drinking water aquifers (DWA), a two-stage approach is taken. First, order of magnitude estimates are made using an analytical model developed to predict single-phase flow from a storage formation into a well, then into a confined aquifer above. Then, the TOUGH2-ECO2N multiphase flow simulator (Pruess, 2007) is used to perform in depth analyses of dissolved CO_2 leakage considering flow effects in and near an abandoned well due to changing pressure, temperature, salinity and gas exsolution.

3. BASE CASE MODELS

3.1 Analytical Model

An analytical model is developed to provide leading order understanding of what parameters in a wellbore leakage system have the largest effect on leakage rates into overlying formations. The solution applies only to single phase, uniform density flow. However, the insights gained from it provide practical results that can be extended to wellbore leakage of brine at the area of review boundary as well as CO_2 laden brine leakage.

A conceptual drawing of the analytical model geometry and parameters is presented in figure 2. These model assumptions represent leakage from a storage formation connected directly to a DWA through a wellbore with no interbedded layers allowing for fluid communication. This simplification is representative of an endpoint case where CO_2 leakage risks to a DWA would be highest.

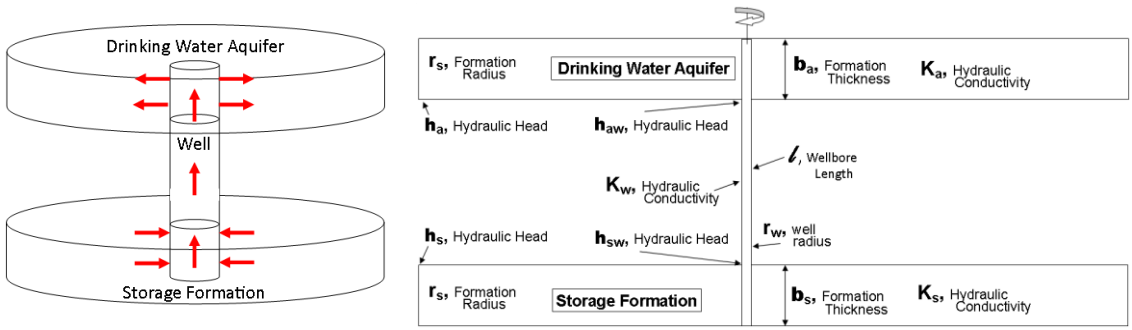

Figure 2: Conceptual Drawing of the analytical model's geometry and parameters. a) Conceptual models with arrows indicating the direction of flow. b) Drawing showing the variables used in the analytical model.

The analytical model is developed by assuming steady state radial flow in a deep storage formation, and a shallower DWA. Flow through the connecting wellbore where it is desired to consider laminar flow through porous media as well as flow through an open pipe, the wellbore is treated in two separate ways. For laminar and turbulent flow in an open or nearly open well, the Darcy-Weisbach equation for open pipe flow is used. The use of an analytical pipe flow model has been suggested in other research (Nordbotten et al. 2005, 2009). Wellbores with substantial blockage due to fill material are modeled assuming laminar flow through porous media according to Darcy's law.

The steady-state volumetric flow rate (Q) into the well from the storage formation is given by (Thiem, 1906):

$$Q_s = 2\pi b_s K_s \left(\frac{[h_s - h_{sw}]}{\ln\left[r_w / r_s \right]} \right) \qquad \textbf{Eq. 1}$$

where Q_s is the flow rate, b_s is the thickness of the storage formation, K_s is the hydraulic conductivity of the storage formation, h_s is the hydraulic head at the radial boundary of the storage formation, h_{sw} is the hydraulic head at the well in the storage formation, r_w is the well radius, and r_s is the radial boundary distance.

Radial flow in the DWA is similarly:

$$Q_a = 2\pi b_a K_a \left(\frac{[h_a - h_{aw}]}{\ln\left[r_w / r_a \right]} \right) \qquad \textbf{Eq. 2}$$

where the subscript *a* indicates the overlying drinking water aquifer.

Freeze & Cherry (1979), suggest that the use of Darcy's law is valid for materials with permeabilities as high as $1x10^{-7}$ m^2, representing a coarse gravel. In addition, the use of Darcy's law in numerical models of wellbore leakage has been used in related studies (Birkholzer et al., 2011; Ebigbo et al., 2007). Therefore, to examine wellbores with permeabilities below $1x10^{-7}$ m^2, the laminar volumetric flow rate in the well is given by:

$$Q_w = \pi r_w^2 K_w \left(\frac{h_{sw} - h_{aw}}{l} \right) \qquad \textbf{Eq. 3}$$

where *l* is the length of the wellbore between the two formations and the subscript *w* denotes the well.

These equations can be rearranged in terms of the head loss:

$$\left(h_s - h_{sw}\right) = \frac{Q_s \ln\left(r_w / r_s\right)}{2\pi b_s K_s} \qquad \textbf{Eq. 4}$$

$$\left(h_a - h_{aw}\right) = \frac{Q_a \ln\left(r_w / r_a\right)}{2\pi b_a K_a} \qquad \textbf{Eq. 5}$$

$$\left(h_{sw} - h_{aw}\right) = \frac{Q_w l}{\pi r_w^2 K_w} \qquad \textbf{Eq. 6}$$

Assuming steady state flow, the magnitudes of Q_s, Q_a, and Q_w are the same. For flow out of the storage formation $Q_s < 0$, while Q_w and Q_a are > 0 as water flows up the well and into the DWA. Letting $Q_s = -Q_a$ and rearranging the log terms in equations 4 and 5:

$$\left(h_s - h_{sw}\right) = \frac{Q_a \ln\left(r_s / r_w\right)}{2\pi b_s K_s} \qquad \textbf{Eq. 7}$$

$$\left(h_{aw} - h_a\right) = \frac{Q_a \ln\left(r_a / r_w\right)}{2\pi b_a K_a} \qquad \textbf{Eq. 8}$$

Adding the three head drops from equations 6, 7 and 8 together gives the total head drop between the formations:

$$\left(h_s - h_a\right) = Q\left(\frac{\ln\left(r_s / r_w\right)}{2\pi b_s K_s} + \frac{l}{\pi r_w^2 K_w} + \frac{\ln\left(r_a / r_w\right)}{2\pi b_a K_a}\right) \qquad \textbf{Eq. 9}$$

or

$$Q = \frac{\left(h_s - h_a\right)}{\left(\frac{\ln\left(r_s/r_w\right)}{2\pi b_s K_s} + \frac{l}{\pi r_w^2 K_w} + \frac{\ln\left(r_a/r_w\right)}{2\pi b_a K_a}\right)} \qquad \textbf{Eq. 10}$$

Equation 10 describes the flow rate of water leaking through an abandoned well due to a head difference between the storage formation and DWA. The flow rate is a function of the head difference between the two formations and the properties of the well and both formations. The term in the denominator is the overall flow resistance of the system.

In terms of well permeability, the assumption of laminar flow according to Darcy's cannot be assumed at permeabilities above $1\text{x}10^{-7}$ m^2. At values above this, the use of a permeability term in the well is somewhat of an abstraction as the well is more akin to an open unobstructed pipe where either laminar or turbulent flow may occur. In order to consider this open condition, the wellbore flow term in equation 6 is replaced with the Darcy-Weisbach equation (Gupta, 2001) which characterizes laminar and turbulent pipe flow:

$$\left(h_{sw} - h_{aw}\right) = \frac{Q_w^2 f l}{4\pi^2 r_w^5 g} \qquad \textbf{Eq. 11}$$

where f is the Darcy-Weisbach friction factor which depends on the Reynolds number and roughness assumptions for the pipe. In addition, g is acceleration due to gravity. Solving for the head drop as in equation 9 results in:

$$\left(h_s - h_a\right) = \left(\frac{f l}{4\pi r_w^5 g}\right) Q^2 + \left(\frac{\ln\left(r_s/r_w\right)}{2\pi b_s K_s} + \frac{\ln\left(r_a/r_w\right)}{2\pi b_a K_a}\right) Q \qquad \textbf{Eq. 12}$$

or

$$Q = \frac{-\left(\frac{\ln\left(r_s/r_w\right)}{2\pi b_s K_s} + \frac{\ln\left(r_a/r_w\right)}{2\pi b_a K_a}\right) + \sqrt{\left(\frac{\ln\left(r_s/r_w\right)}{2\pi b_s K_s} + \frac{\ln\left(r_a/r_w\right)}{2\pi b_a K_a}\right)^2 + 4\left(\frac{f\,l}{4\pi r_w^5 g}\right)\left(h_s - h_a\right)}}{2\left(\frac{f\,l}{4\pi^2 r_w^5 g}\right)} \quad \textbf{Eq. 13}$$

Equation 13 allows for examining a worst-case scenario for wellbore leakage where a well with laminar or turbulent flow is connected directly to a storage formation and a DWA with no fluid interactions with interbedded stratigraphy.

The model parameters used in both analytical and numerical models can be seen in tables 1 &2.

Table 1: Analytical and Numerical Model Parameters

Model Dimensions	
Radial Dimension	R=5,000 m. Due to the use of a fixed boundary condition, this distance assures that flow effect at the radial boundary will be minimal.
Vertical Dimension	Z=1,200 m. The top of the model is set to a depth 200 m below the ground surface. The thickness of both the DWA and Storage Formation are 100 m. They are separated by a 1,000 m impermeable layer. The base of the model is 1,400 m below the ground surface.
Initial Conditions	
Pressure	Hydrostatic equilibrium such that the pressure at the top of the DWA is 2.0×10^6 Pa and 1.4×10^7 Pa at the base of the model.
Temperature	Geothermal gradient of 30°C/km, surface temperature of 15°C. Temperature at upper boundary: 21°C; base of model: 57°C

Table 2: Material Properties for Analytical and Numerical Models		
Property	**Value**	**Comment**
Entire Model		
Thermal Conductivity (W/m·°C)	2.51	Representative of values used in similar studies (Pruess, 2008)
Heat Capacity (J/Kg·°C)	920	
Rock Density (Kg/m^3)	2600	
Drinking Water Aquifer		
Permeability (m^2)	1x10^{-12}	
Porosity	0.25	
Salinity (mg/l)	0	
Impermeable Layer		
Permeability (m^2)	1x10^{-20}	
Porosity	1x10^{-4}	
Storage Formation		
Permeability (m^2)	1x10^{-13}	
Porosity	0.25	
Salinity (mg/l)	20,000	Represents a low salinity brine; this allows for a better examination of effects due to dissolved CO_2 instead of salt. Salinity is varied in subsequent models
CO_2 Mass Fraction	0.044	Represents the maximum CO_2 solubility at the top of the storage formation prior to any change in pressure.
Wellbore		
Permeability, (m^2)	1x10^{-5}– 1x10^{-12}	Varied between models
Porosity	0.98	
Well Diameter (m)	0.2 (8 inch) 0.457 (18 inch) 0.61(inch)	Varied between models

3.1.2 Dimensionless Analysis

In order to quantify the degree to which each parameter controls the overall flow rate of the system, Equation 10 is converted to a non-dimensional form.

$$Q^* = \frac{Q \ln\left(r_s / r_w\right)}{\left(h_s - h_a\right) 2\pi b_s K_s} = \frac{C_w C_a}{\left(C_w C_a + C_w + C_a\right)} \qquad \textbf{Eq. 14}$$

$$C_w = \frac{r_w^2 K_w \ln\left(r_s / r_w\right)}{2 l b_s K_s} \qquad \textbf{Eq. 15}$$

$$C_a = \frac{\ln\left(r_s / r_w\right) b_a K_a}{\ln\left(r_a / r_w\right) b_s K_s} \qquad \textbf{Eq. 16}$$

In equation 14, Q* is the dimensionless flow rate. The term C_w represents the dimensionless flow conductance (the inverse of resistance) provided by the well scaled to the storage formation. Finally, the term C_a represents the dimensionless flow conductance due to the geologic formations. This dimensionless form can be used to analyze what parameters are controlling flow rates for any system being analyzed.

The relationship between dimensionless well and formation conductances is used to determine whether the leakage flow rate in a system is dependent on the wellbore, the geologic formations, or some combination of both. If the wellbore conducts fluid much easier than the geologic formations ($C_w >> C_a$), then the well will only have a minimal effect on the overall flow rate because it provide minimal flow resistance, and Q* will approach 1. Conversely, if the wellbore is much less conductive than the geologic formations (Ca>>Cw), the wellbore will restrict the flow rate in the entire system and Q*<<1. If the wellbore and geologic formations conduct fluid equally, then $C_w = C_a$.

A critical value for well conductance can be used in order to determine when a value for a given parameter will make significantly changes to the flow rate in the system. The

critical well conductance is defined by a chosen reduction in the overall flow rate (R_Q), which ranges between 0-1. The value for the flow rate reduction due to well conductance can be adjusted for any degree of sensitivity. For this research, if the overall flow rate is reduced 10%, then it is assumed that the wellbore is beginning to significantly reduce the flow rate. The critical well conductance (C_{wc}) can be related to the flow rate through:

$$C_{wc} = \frac{1}{R_Q} - 1 \qquad \textbf{Eq. 17}$$

Thus, for the overall flow rate to be reduced 10%, R_Q=0.1 and C_{wc}=9. For the critical well conductance, the value for any parameter related to the wellbore can be calculated using:

$$C_{wc} = \frac{r_w^2 K_w \ln\left(r_s / r_w \right)}{2 l b_s K_s} \qquad \textbf{Eq. 18}$$

and solving for the parameter of interest.

The analytical solution is used in order to develop a first order understanding of how changes in well permeability affect overall leakage through the system. A dimensionless analysis is used in order to determine at what well permeability the well's conductance will significantly reduce the flow rate in the system.

Rearranging equation 18 for hydraulic conductivity in the well and converting to a critical permeability (k_{wc}) gives:

$$k_{wc} = \frac{K_w \mu_w}{\rho_w g} = \frac{2 l b_s K_s C_{wc} \mu_w}{r_w^2 \ln\left(r_s / r_w \right) \rho_w g} \qquad \textbf{Eq. 19}$$

Using the numerical model parameters from tables 1-3, equation 19 predicts that the flow rate will not drop 10% (R_Q=0.1) until the well permeability is below 1.7×10^{-6} m^2, indicating that the wellbore is starting to exert significant control over the leakage rate (figure 3).

As previously discussed, if the conductance of the well is much higher than the geologic formations, it will only minimally reduce the flow rate in the overall system. Because there is a linear increase in well conductance with increasing well permeability in equation 19, this suggests that at well permeabilities indicative of turbulent pipe flow conditions where there is no porous media blocking the well, the wellbore properties may not significantly contribute to the leakage behavior in the system due to geologic formations controlling the overall leakage flow rate.

Furthermore, the analytical solution predicts that at wellbore permeabilities below this critical value, the wellbore conductance (and thus the overall flow rate) will behave such that an order of magnitude decrease in well permeability also decrease conductance by an order of magnitude.

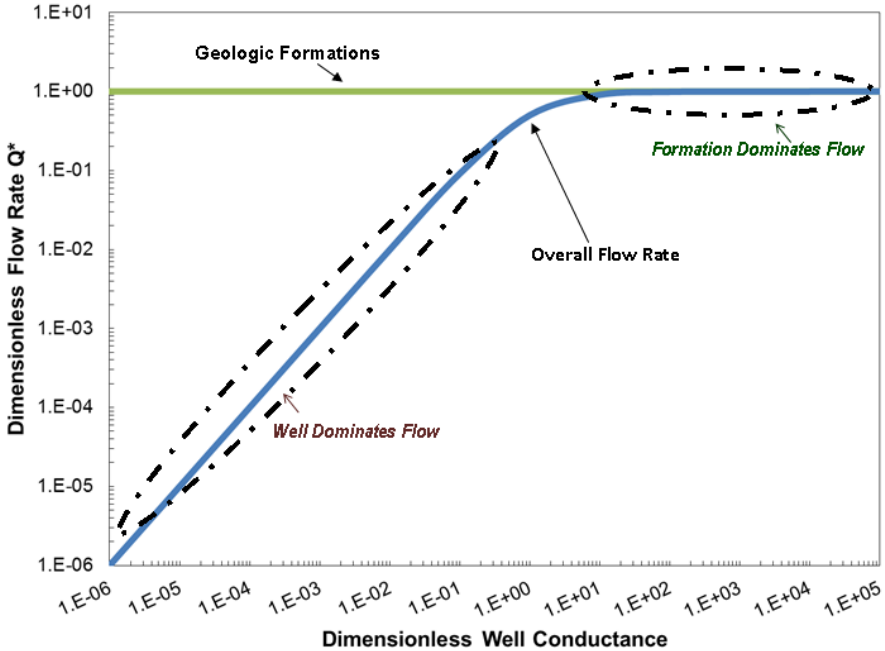

Figure 3: Dimensionless flow rate for the model showing at what well conductances the overall flow rate is controlled by the geologic media or the wellbore.

3.2 Base Case Numerical Model

In order to perform in depth analyses of CO_2 laden brine leakage, it is necessary to consider effects that cannot be accounted for in the analytical solution. To better understand leakage flow rates, it is necessary to not only understand flow effects due to system properties, but also effects due to pressure and temperature gradients, phase change, salinity, and multiphase flow effects.

The numerical model is constructed using the TOUGH2-ECO2N multiphase flow simulator (Pruess, 2007) with the PetraSim GUI (Swenson, D. 2003). The TOUGH2-ECO2N simulator allows for modeling the development of dissolved as well as gaseous

CO_2 plumes in the DWA due to overpressurization of the storage formation or DWA drawdown.

A radially symmetric numerical grid design is utilized for the simulations, which is similar to numerical grids used in other studies (Birkholzer et al., 2011). In figure 4, the model design can be seen. This model represents the same endpoint case as the analytical solution, where a dissolved CO_2 storage formation is directly connected to a DWA through a wellbore. This allows for an evaluation of flow effects with simple, but representative geometry. In addition, it allows for a direct comparison to the results predicted through the analytical solution.

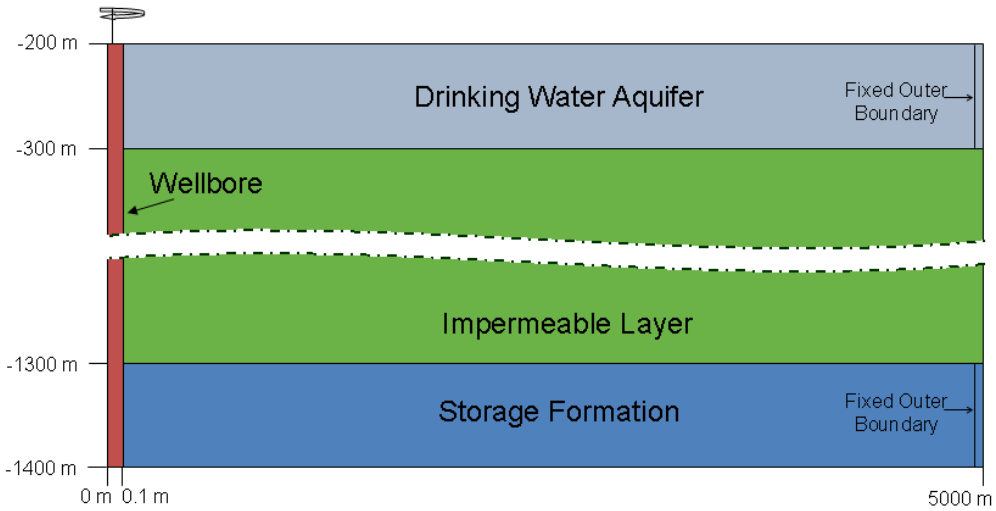

Figure 4: Base case numerical model setup. The storage formation and DWA are separated by a 1000-meter thick impermeable layer. All formations are penetrated by a well in the central radial element.

The outer radius of the model is set to 5,000 meters. This radius contains developing leakage plumes inside the model and is sufficiently large as to minimalize numerical end effects. The model is given an overall vertical length of 1,200 meters. Both the storage

formation and the drinking water aquifer are 100 meters thick. Between the two formations is a 1000-meter thick impermeable layer. The impermeable layer between the formations represents a case where only flow between the storage formation and the DWA are considered. The layer does not transmit fluids, but it does allow for thermal conduction of heat from the warmer storage formation brine as it rises through the wellbore. Finally, the top of the model is set at a depth of 200-meters below the ground surface, which is a representative depth for a large regional DWA (table 1).

Hydrostatic pressure is used to generate the pressure gradient such that the pressure in the top of the upper formation is 2.0×10^6 Pa and the bottom of the lower formation is 1.4×10^7 Pa. A geothermal gradient of 30°C/km with a surface temperature of 15°C is used (table 1). This gradient is typical of the western United States and has been used in other numerical models (Pruess, 2008).

In order to induce overpressure or drawdown within the model, the outermost radial grid block is given a fixed state condition. By either overpressurizing these outer storage formation grid blocks or lowering the pressure in the outer DWA grid blocks, flow through the well is induced.

Differing from the simple analytical model, the numerical model uses permeability (k) which is related to hydraulic conductivity (K) through:

$$k = \frac{K\mu}{\rho g} \qquad \textbf{Eq. 20}$$

where ρ and μ represent liquid density and dynamic viscosity respectively, and g is acceleration due to gravity.

The wellbore is modeled as the central radial element in the model, which is given a different permeability from the surrounding elements. Due to limitations of the numerical simulator, it is assumed that Darcy's law applies to the well as in other studies (Nordbotten et al., 2005; Ebigbo et al., 2007; Nordbotten et al., 2009; Birkholzer et al., 2011). Therefore, when well permeabilities above $1x10^{-7}$ m^2 are used in the numerical simulations, it is assumed they are representative of open pipe flow. While the assumption of laminar flow according to Darcy's law in the wellbore may not fully capture flow effects for the case of turbulent flow or for different multiphase flow regimes in an open wellbore, it does provide valuable results for other cases and useful insights for all cases.

The model is discretized by using 87 grid blocks in the radial dimension. The radial grid blocks are refined around the well with each successive ring increasing in thickness to 95 m. The outermost ring is given a radial thickness of 10 m and is used to impose a fixed state boundary on the model. The fixed state conditions (constant pressure, temperature, salt concentration, CO_2 saturation) in this ring allow for flow into the storage formation as well as flow out of the DWA. Similar to Birkholzer et al. (2011), the pressure in the outer ring can be increased to overpressurize the storage formation or lowered to induce drawdown in the DWA.

In the vertical z dimension, 70 grid blocks are used. The storage formation uses ten 10-meter thick model layers whereas the DWA is refined using twenty 5-meter thick

model layers. The impermeable layer consists of forty 25-meter thick model layers. This discretization results in a total of 6090 grid blocks for the entire model.

The material properties in the model represent typical properties for potential carbon sequestration sites, rather than the properties of a particular location (tables 2 & 3).

Relative permeabilities for gaseous CO_2 and brine are calculated using (van-Genuchten, 1980)

$$k_{rl} = \left(\frac{S_l - S_{lr}}{S_{ls} - S_{lr}}\right)^{\frac{1}{2}} \left(1 - \left[1 - \left(\frac{S_l - S_{lr}}{S_{ls} - S_{lr}}\right)^{1/\lambda}\right]^{\lambda}\right)^2 \qquad \textbf{Eq. 21}$$

$$k_{rg} = \left(1 - \left[\frac{S_l - S_{lr}}{1 - S_{lr} - S_{gr}}\right]\right)^2 \left(1 - \left[\frac{S_l - S_{lr}}{1 - S_{lr} - S_{gr}}\right]^2\right) \qquad \textbf{Eq. 22}$$

where k_{rl} and k_{rg} are the liquid and gas relative permeabilities. S_l, S_{lr}, and S_{ls} are the liquid saturation, residual liquid saturation, and maximum water saturation respectively. S_{gr} is the residual gas saturation and λ is a curve fitting parameter.

Capillary pressure is also calculated using the van Genuchten model:

$$P_c = -P_0 \left(\left(\frac{S_l - S_{lr}}{S_{ls} - S_{lr}}\right)^{\frac{-1}{\lambda}} - 1\right)^{1-\lambda} \qquad \textbf{Eq. 23}$$

The relative permeability and capillary pressure parameters used in the model are derived from simulations in Doughty, (2007).

Table 3: Relative Permeability and Capillary Pressure Parameters for Base Case Model				
Relative Permeability van Genuchten-Mualem Model	**λ**	**S_{lr}**	**S_{gr}**	**S_{ls}**
All Rock Units	0.412	0.3	0.125	1
Wellbore	0.412	0.02	0.02	1
Capillary Pressure van Genuchten Model	**λ**	**S_{lr}**	**P_0 (kPa)**	**S_{ls}**
All Rock Units	0.412	0.3	13.3	1
Wellbore	Zero Capillary Pressure			

For the wellbore, it is desired to minimalize relative permeability and capillary pressure effects. Therefore, the relative permeability parameters for the well are changed so that S_{lr} and S_{gr} are both 0.02. Capillary pressure is zero in the well. In addition, the well porosity is set to 0.98.

Because the numerical model is used to evaluate the effects of a suite of different parameters, the well's permeability and diameter vary between simulations. In addition, simulations are run with different values for storage formation salinity as well as for different distances between the DWA and storage formation. System overpressures and drawdowns range between 10-30 bar.

3.3 Comparison of Analytical and Numerical Models

For this comparison, the numerical model described in section 3.2 is modified slightly such that the impermeable layer is removed. In addition, the temperature is set to a uniform 35°C, salt and CO_2 is removed, and the model is run isothermally. A 8-inch diameter $1x10^{-8}$ m^2 permeability well is used for both the analytical and numerical models. All other system parameters from the numerical model are used to calculate the analytical solution. This allows for a simple direct comparison between the analytical

solution and numerical simulations. The volumetric flow rates predicted by the analytical model are then compared to the numerical simulation for consistency.

The first comparison is the sensitivity of the flow rate to changes in well permeability. In the numerical model, the bottom storage formation is given an overpressure of 20 bar to induce flow up the well. Once steady state is obtained, the volumetric flow rates predicted by the analytical model are compared to numerical simulations (table 4). For well permeabilities at and below $1x10^{-8}$ m^2, where fluid flow is laminar and obeys Darcy's law (Freeze & Cherry, 1979), the numerical and analytical flow rates match within 2% of each other.

At high well permeabilities for the analytical flow rate using equation 10, as well as the numerical simulations, the assumption of laminar flow through porous media is no longer valid. The predicted flow rates for a $1x10^{-6}$ m^2 permeability wellbores are in the turbulent flow regime, assuming a completely open pipe (Reynolds # $\approx 1.0x10^5$). Because the analytical solution using equation 10 cannot account for resistance due to turbulent flow, it slightly overpredicts flow rates at high permeabilities.

Using the analytical solution that assumes turbulent flow using the Darcy-Weisbach equation, the predicted flow rate in the system is lower due to friction from turbulent flow in the pipe. Although the numerical simulations still assume laminar flow, there is a reasonable match between the flow rate it predicts and the turbulent flow calculation.

Table 4: Model Validation Showing Well Permeability vs. Flow Rate				
Well Permeability (m^2)	**Analytical Flow Rate Eq. 10 (m^3/s)**	**Analytical Flow Rate Eq. 13 (m^3/s)**	**Numerical Flow Rate (m^3/s)**	**Variation from Eq. 10**
$1.0x10^{-12}$	$8.664x10^{-8}$	-	$8.794x10^{-8}$	1.5%
$1.0x10^{-10}$	$8.659x10^{-6}$	-	$8.769x10^{-6}$	1.3%
$1.0x10^{-8}$	$8.178x10^{-4}$	-	$8.035x10^{-4}$	1.8%
$1.0x10^{-6}$	$1.249x10^{-2}$	-	$1.222x10^{-2}$	2.2%
$1.0x10^{-4}$	$1.456x10^{-2}$	$1.425x10^{-2}$	$1.423x10^{-2}$	2.3%

The analytical flow rates from equation 10 over a range of wellbore permeabilities are compared to the flow rate from equation 13 (figure 5). At high well permeabilities (> $1x10^{-6}$ m^2), equation 10 that assumes laminar flow according to Darcy's law reasonably approximates the flow predicted for the open turbulent flow case. The numerical model is also reasonably accurate. This is applicable to later comparisons between the analytical solution and numerical simulations. In subsequent numerical models, it is assumed that Darcy's law is still valid at well permeabilities as high as $1x10^{-8}$ m^2. Other researchers have made similar assumptions (Birkholzer, J.T. 2011).

For instances where higher well permeabilities above $1x10^{-8}$ m^2 are modeled numerically, although the permeability term is used in the wellbore, the system is thought of as if the wellbore is functioning as an open pipe with turbulent flow. The numerical flow rates likely overpredict leakage rates because the numerical model cannot account for pipe friction due to turbulent flow not does it consider effects of open pipe multiphase flow regimes. In addition, between $1x10^{-8}$ m^2 and $1x10^{-6}$ m^2 well permeabilities, the transition from laminar flow through porous media to open turbulent pipe flow occurs. In

the numerical models, it is assumed that permeabilities of $1x10^{-6}$ m^2 and higher represents fully established turbulent flow in the wellbore.

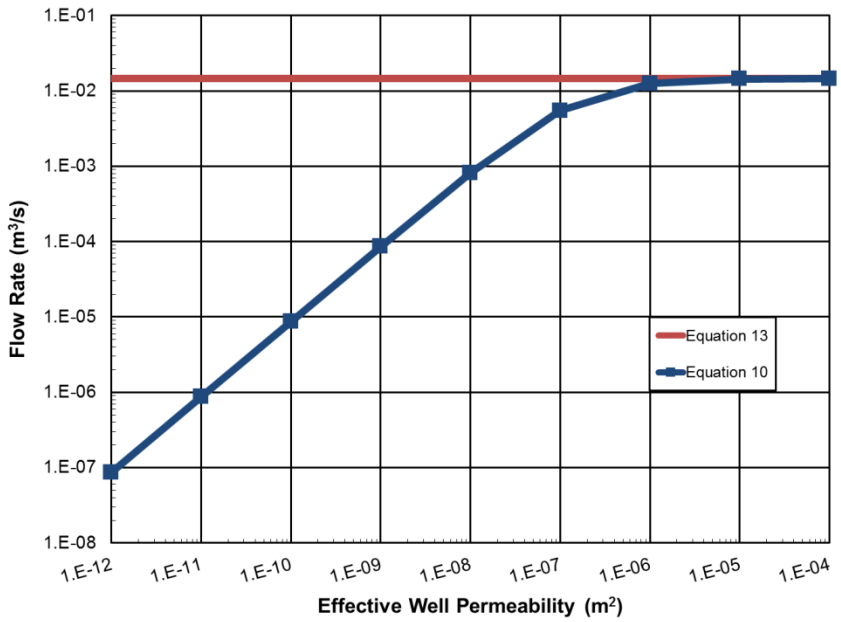

Figure 5: Comparison of the laminar and turbulent flow analytical solutions for a range of well permeabilities. Laminar flow in the wellbore under Darcy's law from equation 10 converges to the turbulent Darcy-Weisbach pipe flow from equation 13 at well permeabilities higher than $1x10^{-6}$ m^2 for parameters used in subsequent numerical simulations.

A second comparison is performed at three different storage formation overpressures. An 8-inch $1x10^{-8}$ m^2 permeability well is used where laminar flow in the well is still valid. For all overpressures, the analytical and numerical models both predict flow rates that are within a few percent of each other (table 5). Therefore, there is good agreement between the numerical and analytical models.

Table 5: Model Validation of Overpressure vs. Flow Rate			
Overpressure (bar)	**Analytical Flow rate (m^3/s)**	**Numerical Flow rate (m^3/s)**	**Variation**
10	4.069×10^{-4}	3.930×10^{-4}	3.4%
20	8.178×10^{-4}	8.035×10^{-4}	1.8%
30	1.229×10^{-3}	1.199×10^{-3}	2.4%

The simple analytical solutions produce results that are consistent with numerical models for single phase, uniform density flow. However, they can only approximate the actual flow rate for cases of dissolved CO_2 wellbore leakage because dissolved CO_2 leakage involves significant transient effects. However, it is useful in predicting leading order behavior and the expected relationship between leakage flow rates and system parameters.

3.4 Flow Effects Due to Changing Well Permeability

The first scenario studied is the effect of wellbore permeability on CO_2 laden brine leakage rates into a drinking water aquifer (DWA). As seen in the uniform density case (table 4), volumetric flow rates vary over more than five orders of magnitude with changes in well permeability. At well permeabilities similar to that of aquifers, the leakage flow rate is reasonably small at 2 gallons/day. However, for turbulent pipe flow, up to 230 gallons/minute of leakage is calculated analytically.

Knowing the apparent permeability of an improperly abandoned well is difficult since so little is known about the spatial distribution and properties of these wells (Ide et al., 2006). Similar to this study, other researchers have dealt with leaky wellbore

permeability by using a range of permeability values (Celia et al., 2004; Birkholzer et al., 2011).

To investigate wellbore leakage of CO_2 laden brine, numerical simulations are conducted using the model from section 3.2. The leakage due to various well permeabilities is then compared to analytical predictions from section 3.4.1. This numerical model uses an 8-inch (0.2 m) diameter well and the storage formation is overpressurized 20 bar to induce flow up the wellbore. This overpressure is consistent with predicted long-term overpressures seen in other studies (Zhou et al., 2010).

In the wellbore, a significant fraction of the CO_2 exsolves to form a separate gas phase as the brine is depressurized. Simulations show that this gas phase first appears near the top of the wellbore. Because of opposing effects on CO_2 solubility between temperature and pressure, under static conditions, exsolution is expected to be depressed until well above the critical point for CO_2, Furthermore, for overpressurization, pressure will increase along the wellbore. This initial effect serves to make the solubility of CO_2 increase at shallower depths in the wellbore. Over time, as the leakage of CO_2 laden brine is fully established, the column of exsolving gas in the wellbore moves downward due to an overall increase in temperature in and around the wellbore. This temperature increase is due to the leaking brine being warmer than resident fluids. The primary pressure effects and secondary thermal effects on solubility can be seen in figure 6.

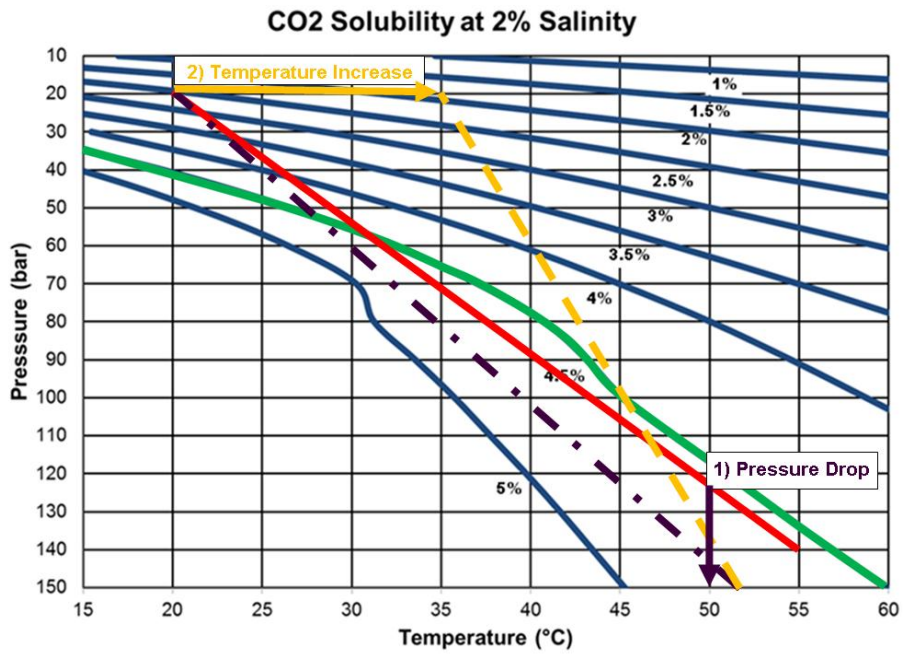

Figure 6: Changing solubility of CO_2 in the wellbore with changes in pressure and temperature. For parameters from the numerical model, initial static conditions suggest exsolution will not occur until 60 bar (-600 m) is crossed by the leaking brine. Increasing pressure allows the con to stay in solution until 50 bar (-500 m). Over time, thermal effects increase temperature in the wellbore. This decreases solubility along the wellbore such that exsolution occurs at 100 bar (-1000 m)

Table 6 compares the simulated gaseous fraction of the CO_2 plume in the DWA to the equilibrium gas fraction that should exist between the P/T/S conditions of the storage formation and DWA. The equilibrium condition is calculated using ECO2N to establish the solubility of CO2 at the P/T/S conditions of the storage formation and DWA. The difference in these solubilities describes the mass fraction of CO2 that can exsolve.

For leakage simulations at high well permeabilities, the gas fraction exsolved is higher than for leakage with lower well permeability. However, for all simulated cases, less gas has exsolved than is expected from equilibrium calculations (table 6).

Higher gas fractions at high well permeabilities are due to a larger increase in temperature in and around the wellbore. Because flow rates are largest at high permeabilities, more warm brine leaks which heats up the system and reduces CO_2 solubility. Re-dissolution of the exsolving CO_2 as it contacts resident fluid during leakage also reduces the gas phase. At lower well permeabilities, and thus flow rates, this effect becomes dominant. Whenever flow rates are low due to low well permeability, all of the exsolving gas becomes redissolved into the aquifer during leakage.

Table 6: Gas Phase Fraction in DWA Compared to Equilibrium Values

	Well Permeability (m^2)				
	$1.0x10^{-4}$	$1.0x10^{-6}$	$1.0x10^{-8}$	$1.0x10^{-10}$	$1.0x10^{-12}$
Gaseous Fraction of Total CO2 Plume in DWA	19.3%	19.8%	11.4%	0.58%	0.0%
Equilibrium Predicted Gas Fraction	23.8%				

After 50 years of wellbore leakage into the DWA, CO_2 leakage plumes have significantly different magnitudes for cases of different leaky wellbore permeabilities. For well permeabilities below $1x10^{-8}$ m^2, plume magnitudes decrease linearly with decreasing well permeability. However, in simulations with well permeabilities above $1x10^{-7}$ m^2, leakage plumes do not continue to increase in magnitude significantly.

These plumes suggest that at lower well permeabilities, as expected from the analytical solution, the wellbore provides the most resistance to flow. However once the

well provides little resistance to flow, the geologic material dominates and restricts the leakage rate.

The leakage plumes for all well permeabilities have two separate regions. Along the top of the DWA, a gaseous plume occurs which increases in size with increasing well permeability. Secondly, there is a wedge shaped dissolved plume that extends downward to the base of the DWA. It also increases with increasing well permeability.

The gaseous plume spreads along the top of the aquifer due to being highly buoyant compared to the surrounding water. The wedge shaped dissolved plume migrates downward in the DWA because the CO_2 laden brine that is leaking has a higher density than surrounding waters. The dissolved and gaseous leakage plumes in the DWA after 50 years can be seen in figure 7.

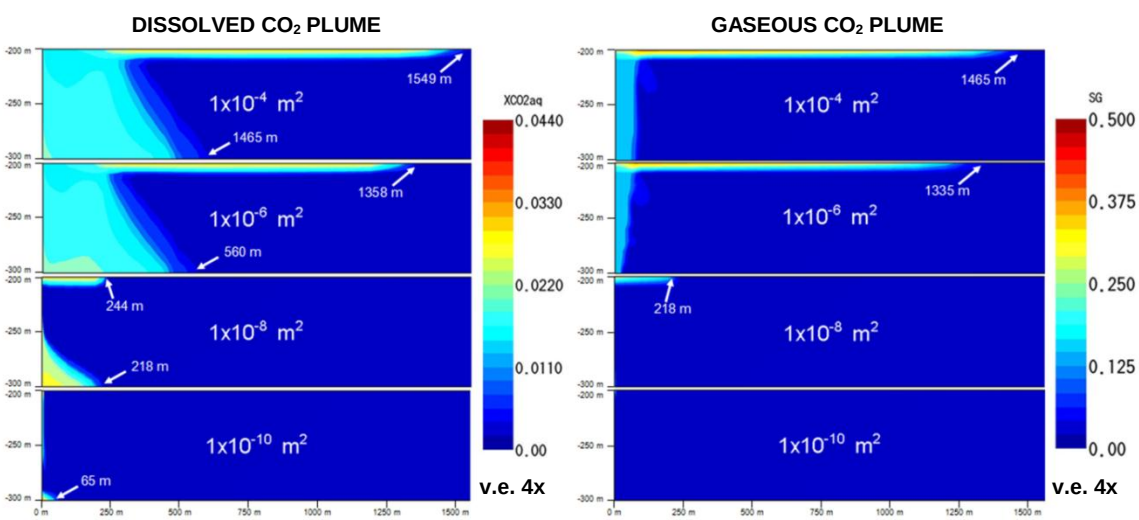

Figure 7: Dissolved and gaseous CO_2 plume in the drinking water aquifer at various well permeabilities at 50 years. Well permeabilities are not shown where plume formation is not significant.

The total CO_2 mass flow rate (dissolved and gaseous) in the well at the base of the DWA over 50 years for well permeabilities ranging between $1x10^{-4}$ to $1x10^{-12}$ m^2 are examined and can be seen in figure 8. At higher well permeabilities ($1x10^{-4}$ to $1x10^{-6}$ m^2), the flow rates are fully established within 3 months. However, as well permeability decreases, the timescale for fully established flow is increased indicating that it takes longer for leaked brine to flow upward at lower permeabilities.

At well permeabilities above $1x10^{-7}$ m^2, the flow rates never reaches steady state but instead exhibits oscillations as well as a slow decline over time. This is due to thermal effects similar to those shown by Oldenburg and Rinaldi, (2010), where warm brine cools upon entry into the DWA and moves downward due to an increase in density. In addition, cooling occurs due to gas exsolution. As wellbore permeabilities below $1x10^{-7}$ m^2, leakage rates of CO_2 reach a steady state once fully established.

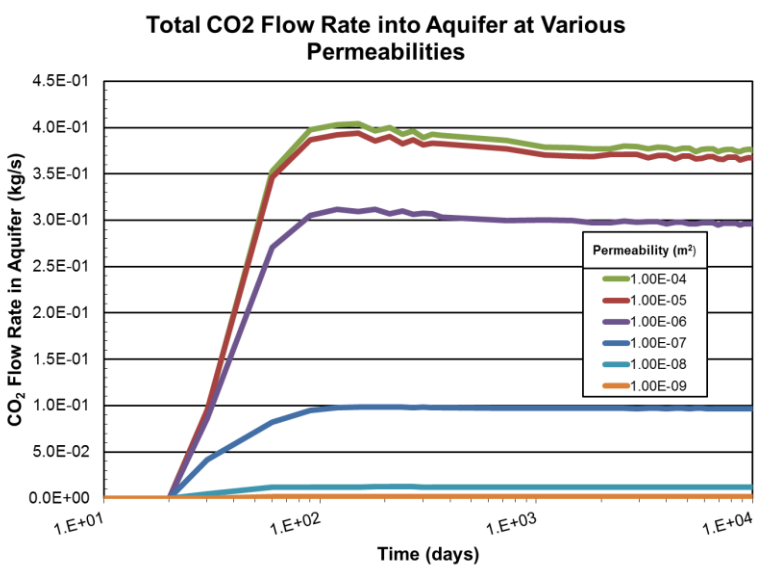

Figure 8: Total CO_2 flow rate into the DWA at various well permeabilities.

At fifty years of leakage, the relationship between well permeability and CO_2 laden brine leakage rates are compared to predicted steady state flow rates from the analytical solution (figure 9). In the numerical simulations, the leakage rate drops linearly with well permeability for permeabilities below $1x10^{-7}$ m^2 . This is consistent with analytical predictions where due to laminar flow through porous media, the resistance to flow in the wellbore limits the leakage rate of the entire system. This linear relationship between well permeability and brine leakage is also consistent with results from Birkholzer et al., (2011).

At simulated well permeabilities above $1x10^{-6}$ m^2 where turbulent flow in the wellbore is assumed to be represented, the flow rate of brine no longer increases linearly with increasing well permeability. Instead, the flow rate begins to approach a maximum. This is consistent with the predictions from the dimensionless analysis, where it was shown that well permeabilities above $1.7x10^{-6}$ m^2, the wellbore would no longer significantly limit flow.

The simulated flow rates from the numerical models are all lower than the analytical predictions for all well permeabilities (figure 9). Because the CO_2 laden brine has a higher density than pure water, the flow rate of brine is lower than pure water due to the increased pressure needed for the denser brine to flow upward. In addition, exsolution of gaseous CO_2 in the wellbore impedes the flow of brine, lowering the effective permeability of the system.

For high well permeabilities, the numerical simulations still use Darcy's law for flow in the wellbore. This assumption ignores flow resistance due to turbulent flow in the pipe

at high Reynolds numbers. It also cannot adequately predict flow resistance in an open pipe due to multiphase flow regimes. This limitation of the numerical simulator may result in overprediction of the leakage simulated for permeabilities meant to represent open pipe flow. Despite these limitations, it is reasonable to surmise that at open wellbore conditions, the well will provide far less resistance to flow than the geologic formations, indicating minimal control over the system. For the parameters from the numerical simulations, using the entire range of friction factors from the Moody diagram(0.1-0.006) in the pipe flow analytical model results in less than a 3% change in flow rate. This suggest that even accounting for resistance due to turbulent flow, the geologic formations will provide an upper limit to the leakage rates of CO_2 laden brine.

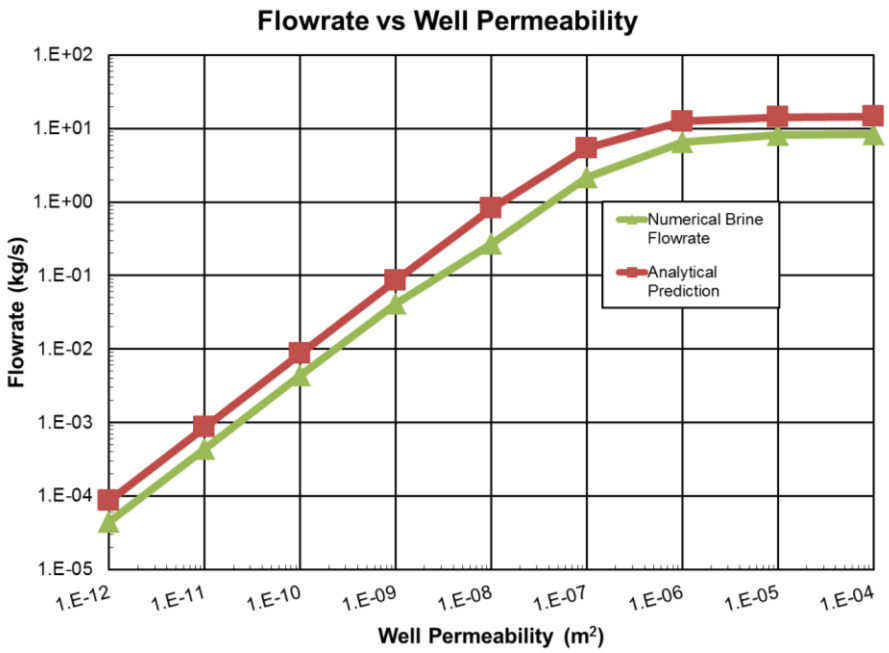

Figure 9: Steady-state aqueous flow rate at various well permeabilities for both the numerical and analytical models.

In order to evaluate the mass of CO_2 that leaks into the DWA as a function of well permeability and storage formation overpressure, many leakage simulations are performed (figure 10). After 25 years, the mass of leaked CO_2 ranges from zero at low permeabilities and overpressures to as much as 0.5 Mt for permeabilities meant to represent leakage through an open pipe.

Although a large mass of CO_2 leaks for the open well cases, this likely represents a worst-case scenario. Leaky well permeability ranges that are probably more realistic in real geologic systems, such as $1x10^{-10}$ to $1x10^{-14}$ m^2, have been used in other studies of wellbore leakage (Celia, M.A. 2004; Nordbotten, J.M. 2005; Nordbotten, J.M. 2009). For this permeability range, the mass of CO_2 leaked is at least three orders of magnitude lower than for open pipe flow leakage. Therefore, leaky wells with some degree of blockage likely pose a lower leakage risk than for leakage through an open pipe.

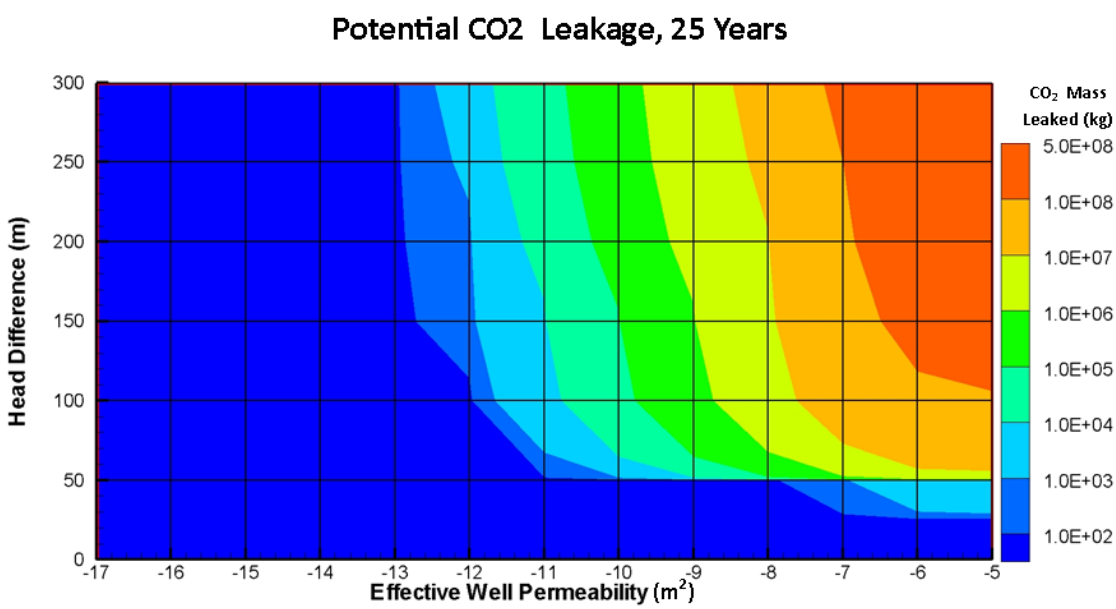

Figure 10: Simulation results showing the simulated mass of CO_2 leakage plumes in the DWA as a function of well permeability and formation overpressure.

3.5 Flow Effects Due to Changing Wellbore Diameter

In addition to permeability, the well diameter can have a major effect on the conductance of the well. A range of well diameters are possible, considering that abandoned oil and gas production wells, exploration wells, and monitoring wells are all possible pathways present at most geologic storage locations. All of these have the potential to be improperly sealed and thus provide a leakage pathway (Gass et al., 1977).

In the dimensionless equation 18, it can be seen that increasing well radius can also increase the conductance of the well. However, the effect that well diameter will have on conductance is dependent on the rest of the properties in the system. For different well diameters, the conductance of the well may still be much higher than the geologic media if, for instance the permeability is still high. For the numerical model parameters, if the well is highly permeable ($>1x10^{-6}$ m^2), representing turbulent pipe flow, then equation 18 predicts that the well radius will have to be smaller than 0.04 m (~1.5-inches) in order for the well to provide enough friction to reduce the leakage rate by 10%. Therefore, the effects of well diameter should be minimal for high permeabilities in the numerical models of CO_2 laden brine leakage. Depending on whether equation 10 or 13 is used, the flow effects at small diameters are slightly different due to turbulent friction effects in the pipe flow model.

Once well permeabilities are low enough that laminar flow through porous media in the well limits the conductance of the entire system, changes in well diameter reduce the conductance of the well. For the parameters from the numerical models and well

permeabilities below $1x10^{-8}$ m^2, the analytical solution predicts that an increases in well cross sectional area causes a linear increase in flow rate for realistic well diameters.

To analyze the effect of well diameter on CO_2 laden brine leakage, the ECO2N model is used with the same properties described in section 3.2. However, the innermost radial grid block is adjusted so that well diameters of 8, 18, and 24 inches can be modeled. The model is given a storage formation overpressure of 20 bar for the three well diameters. In addition, two well permeabilities of $1x10^{-8}$ and $1x10^{-5}$ m^2 are simulated.

As calculated analytically, the numerical model shows a linear relationship between the well cross sectional area for the $1x10^{-8}$ m^2 well permeability simulations. Therefore, the brine leakage rate using the 24-inch well is nearly and order of magnitude higher than for the 8-inch well (figure 11).

For the high well permeability simulations, the increase in flow rate with well cross sectional area is greatly reduced. As expected from the analytical solution, whenever the well's permeability is high it provides only minor resistance to the flow of brine.

Comparing the flow rates from the numerical simulations to the analytical values, the flow rates are lower than the analytical values (figure 11) as seen in previous simulations. Once again, this flow reduction is due to the presence of dense CO_2 laden brine in the numerical models.

Examining the CO_2 leakage plumes that develop in the DWA at 50 years for each of the $1x10^{-8}$ m^2 permeability wellbore diameter cases, the gas fraction of each individual plume increases with well diameter. As the flow rate increases, so does the amount of heat and salt that enters the DWA, this in turn lowers the solubility of the CO_2, allowing

more gas to exsolve. Because neither the numerical or the analytical models are able to account for multiphase flow regimes in an open pipe at turbulent flow conditions, it is possible that well diameter may have a larger effect than what is seen in the current simulations for open pipe conditions.

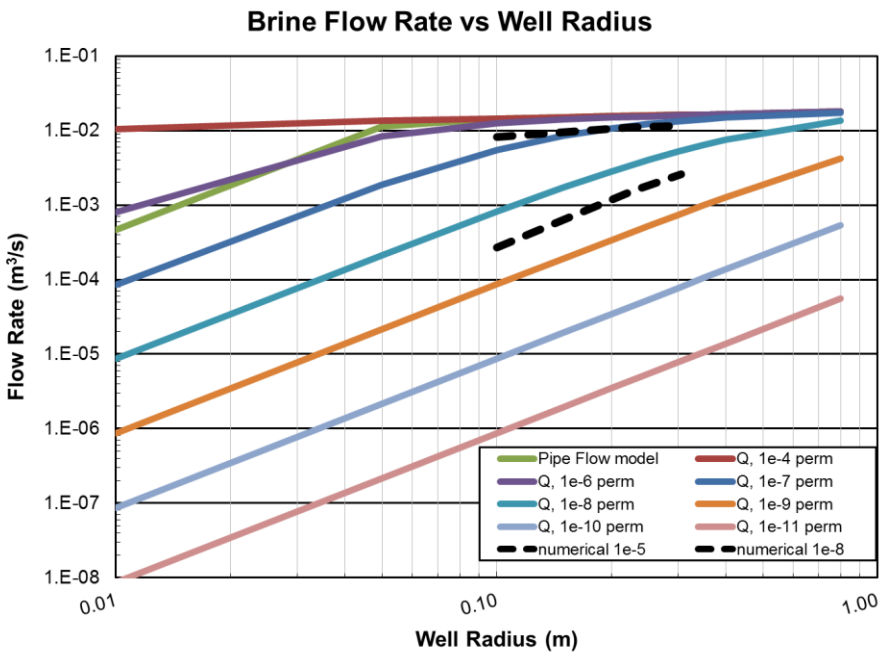

Figure 11: Numerical and analytical aqueous flow rates as a function of changing well radius at several wellbore permeabilities.

3.6 Flow Effects Due to Salinity

Previous studies have shown that when the salinity of the storage formation is increased, the flow rate due to overpressure is decreased (Birkholzer et al., 2011). This is due to fluid density increases with increasing salinity of water. Birkholzer et al. (2011) showed through a static pressure balance equation as well as through numerical

simulations that the threshold overpressure necessary to induce sustained flow up a wellbores increases with salinity. As brine flows up a wellbore, the density of the fluid column has an effect on the leakage rate. Therefore, at a higher salinity and thus higher fluid density, the water flowing up the wellbore is heavier. Because there is more weight, more pressure head is needed to maintain the same flow rate as brine density increases. Thus, whenever the formation overpressure is held constant, the result is a drop in flow rate with increasing brine density.

Whenever CO_2 is dissolved into the brine, it results in an additional increase in brine density. Furthermore, the higher the solubility of the CO_2, the greater the density increase over pure resident brine will be. CO_2 laden brine will therefore always have a higher density than the original resident brine prior to dissolution. It is to be expected that at a given overpressure, there will be a reduction in the leakage flow rates between resident brine and the CO_2 laden brine.

To quantify how much more the addition of CO_2 to brine depresses the flow rate up a wellbore, the model from section 3.2 using an 8-inch diameter $1x10^{-8}$ m^2 permeability well is adjusted to accommodate different salinities. In addition to the original 20,000 mg/l case, 150,000 mg/l, and 260,000 mg/l brines in the storage formation are modeled. At each of these salinities, models are run without CO_2 and with CO_2 dissolved at its maximum solubility for the given pressure, temperature, and salinity conditions at the top of the storage formation prior to overpressure.

The simulated brine flow rates with 30 bar of overpressure for different salinities are compared (figure 12). The flow rate is higher whenever salinity (and fluid density) is

lower. In addition, whenever CO_2 is added, the flow rate is significantly reduced. At lower salinities, where the solubility of CO_2 is greatest, the flow rate is reduced by ~60% with the addition of CO2.

Although this large reduction in flow occurs when CO_2 is dissolved in the brine, density alone cannot explain the effect. For the 2% salinity case, the addition of CO_2 only increase brine density by ~1%. Whenever more CO_2 is present in the leakage system, there is a greater potential for gaseous CO_2 exsolution to impede the flow of brine in the wellbore. This effect causes the large reductions in flow rate seen in the simulations.

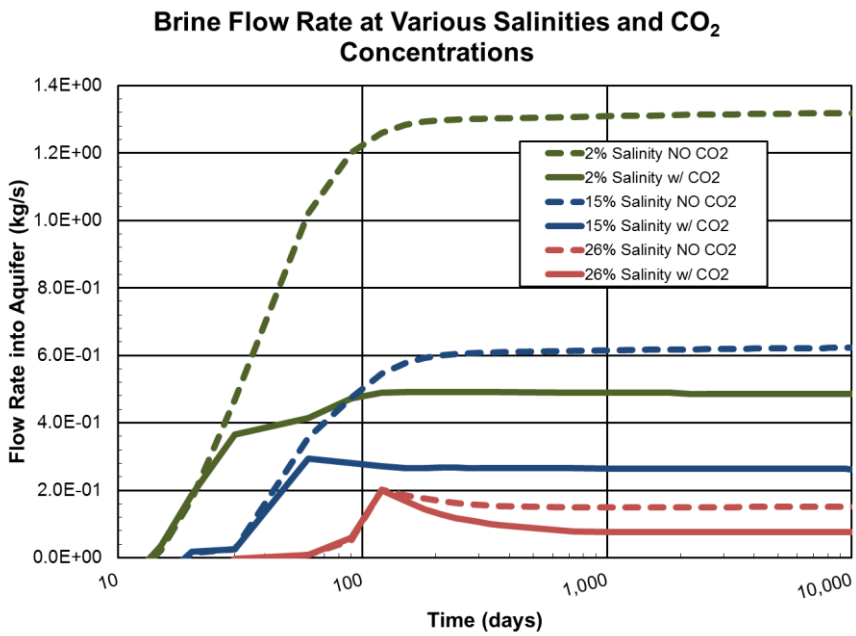

Figure 12: Brine flow rate into the DWA at various salinities with and without dissolved CO2

3.7 Flow Effects Due to Various Overpressures and Drawdowns

When evaluation how CO_2 laden brine may be forced through a leakage pathway, two basic cases must be considered. In order for the fluid to move upward through a wellbore, a change in head gradient must be induced through either storage formation overpressure, or overlying formation drawdown.

Equation 10 suggests a linear relationship between the change in hydraulic head and flow rate. From the analytical solution, increasing the overpressure from 10 to 20 and 30 bar should double and triple the flow rate, respectively (table 5). By comparing the numerical flow rates, the effect of overpressure on CO_2 laden brine leakage can be deduced.

So that overpressure can be compared directly to drawdown in numerical simulations, the numerical model from section 3.2 is manipulated such that the impermeable layer and well length is halved to a thickness of 500 m. This brings the aquifer at the top of the model down to a depth of 700 m below the ground surface while maintaining the storage formation at a depth of 1400 m. This adjustment allows for drawdown of the overlying formation. While this depth no longer is representative of a DWA, the data from the simulations is still applicable for leakage into shallower aquifers. All other model properties are maintained.

3.7.1 Overpressure Effects

Simulations are performed for storage formation overpressures of 10, 20, and 30 bar at well permeabilities of $1x10^{-8}$ and $1x10^{-5}$ m^2 for both the 1000 m and 500 m wellbore

models. The flow rates in the numerical models are all higher than the doubling and tripling expected analytically. In addition, the increases vary between the different cases of wellbore length. Although actual flow rates are higher at increased permeability, the relationship between CO_2 laden brine flow rates and the degree of overpressure shows only a minor dependence on well permeability in the simulations.

The largest flow rate increase is seen with the 1000 meter wellbore. Instead of the analytical predicted doubling and tripling, the simulated flow rates actually increases ~3x when the overpressure is doubled from 10 to 20 bar. Whenever overpressure is tripled from 10 to 30 bar, the flow rate increases ~6x. For the 500 m wellbore models, doubling and tripling the overpressure results in flow rate increases closer to analytical predictions, with increases of ~2.5 to ~3.5x.

These higher than expected flow rate increases compared to analytical predictions are due to fluid density effects. For uniform density flow, any deviation from the static head gradient will induce flow. Considering a higher density brine in the storage formation, overpressurization will induce brine to move up the wellbore. However, sustained leakage of brine will not occur without a pressure threshold being crossed that allows the brine to migrate far enough upward to enter the overlying DWA (Nicot, 2009). In the simulations, the initial 10 bar of overpressure is only slightly above this pressure threshold. Therefore, the flow rate contrast is greater between 10 bar of overpressure and the two subsequent overpressure. Looking at the differences in flow rate for the 20 and 30 bar cases, which are well above the pressure threshold, flow rate increase are close to the analytically predicted doubling. Examining results from other studies shows that

similar increases in flow rate due to overpressure have been observed (Birkholzer et al., 2011). In table 7, the simulation results of various storage formation overpressures can be seen.

Table 7: Numerical Flow Rates Due to Overpressure					
	10 bar	**20 bar**	**Flow Rate Increase**	**30 bar**	**Flow Rate Increase**
$1x10^{-8}$ Permeability					
Flow rate (kg/s) 500 m wellbore	$3.3x10^{-1}$	$8.2x10^{-1}$	**2.5**	1.4	**4.1**
Flow rate (kg/s) 1000 m wellbore	$7.7x10^{-2}$	$2.7x10^{-1}$	**3.5**	$4.9x10^{-1}$	**6.3**
$1x10^{-5}$ Permeability					
Flow rate (kg/s) 500 m wellbore	4.8	11.0	**2.3**	17.0	**3.5**
Flow rate (kg/s) 1000 m wellbore	2.4	8.2	**3.3**	13.7	**5.6**

3.7.2 Drawdown Effects

In order to compare any differences in flow rate between storage formation overpressure and drinking water aquifer drawdown, the 500 m wellbore model explained in 3.7.1 is used. For comparison to the overpressure model, 10, 20, and 30 bar of drawdown are induced for an 8-inch well of permeability $1x10^{-8}$ m^2.

For all three drawdowns, fluid begins to flow up the wellbore within three days of the drawdown being induced. However, for the overpressure case, upward flow does not begin until 20 days after overpressure begins. Although flow begins quickly for drawdown, there is a sharp drop in flow rate within the first few days followed by an

eventual recovery and rise in flow rate. This same drop and recovery also occurs for the overpressure case, but it is not as pronounced. These flow rates can be seen in figure 13.

Upward flow in the well begins faster for drawdown for two reasons. First, because the permeability in the DWA is higher than for the storage formation, the pressure front due to drawdown reaches the wellbore faster than the pressure front due to overpressure reaches the well. In addition, only a small pressure threshold has to be overcome in order for flow to begin due to drawdown. Instead, the lower density fluid in the upper portion of the wellbore is quickly pulled upward. However, when the sharp drop in flow rate occurs, this is indicative of the denser CO_2 laden brine inundating the length of the wellbore. Because this brine is denser, the flow rate drops sharply before eventually recovering to an established flow rate. For overpressure, the drop in flow also occurs because the weight of the fluid column in the well is initially lower until the brine completely inundates the entire length of the wellbore.

As can be seen in figure 13, the established flow rates due to overpressure are higher than for drawdown for all pressure differentials. For the 10 bar case, the flow rate due to overpressure is only slightly higher than for drawdown (13%). Furthermore, for 30 bar the flow rate due to overpressure is 34% higher with the twenty bar case falling in between with a 25% difference.

However, examining the gaseous CO_2 flow rates for all cases, a larger gas phase occurs for drawdown which flows faster. Conversely, to brine flow, the established flow rates of gas are higher in all cases of drawdown compared to overpressure. This can be seen in figure 14.

Since gaseous flow rates are higher due to overpressure, this indicates that more CO_2 is exsolving due to drawdown than overpressure. Because drawdown requires a lowering of pressure in the wellbore compared to an increase from overpressure, the solubility of CO_2 is lower for drawdown. Therefore, as the CO_2 moves upward during drawdown, more gas exsolves, and gaseous flow rates are higher. Although comparatively more gas is exsolving, this effect serves to lower the overall leakage of CO_2 laden brine in the system. As more gas is present, it blocks pore space and impedes the flow of brine. This lowers the effective permeability of the brine and has the overriding effect of lowering the leakage rate of CO_2. Although less total CO_2 leaks due to drawdown, a higher fraction of the total CO_2 leakage plume does occur as a gaseous phase. For leakage through an open wellbore where various multiphase flow regimes occur, flow behavior could be significantly different and the exsolution of more CO_2 may not impede and reduce leakage.

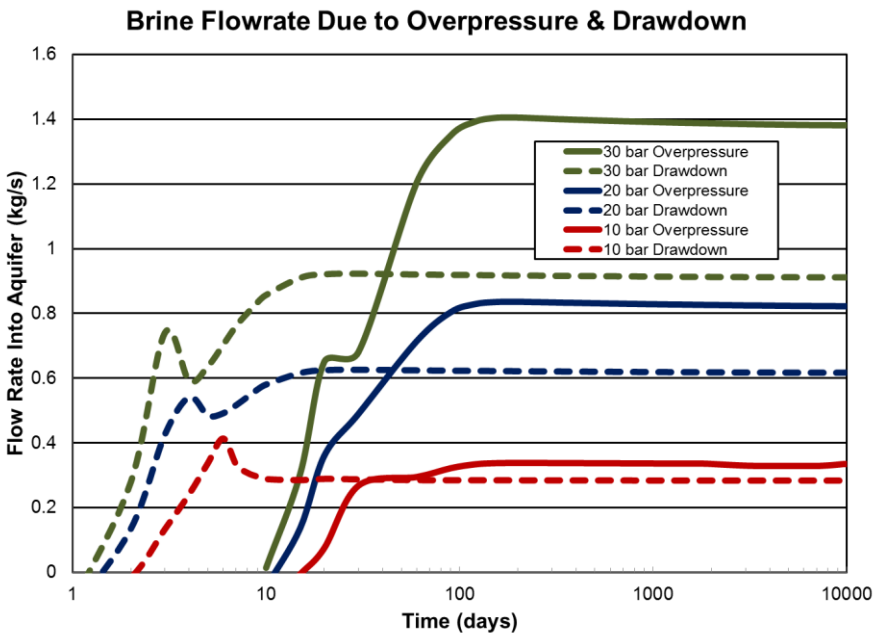

Figure 13: Brine flow rate into the DWA at various overpressures and drawdowns.

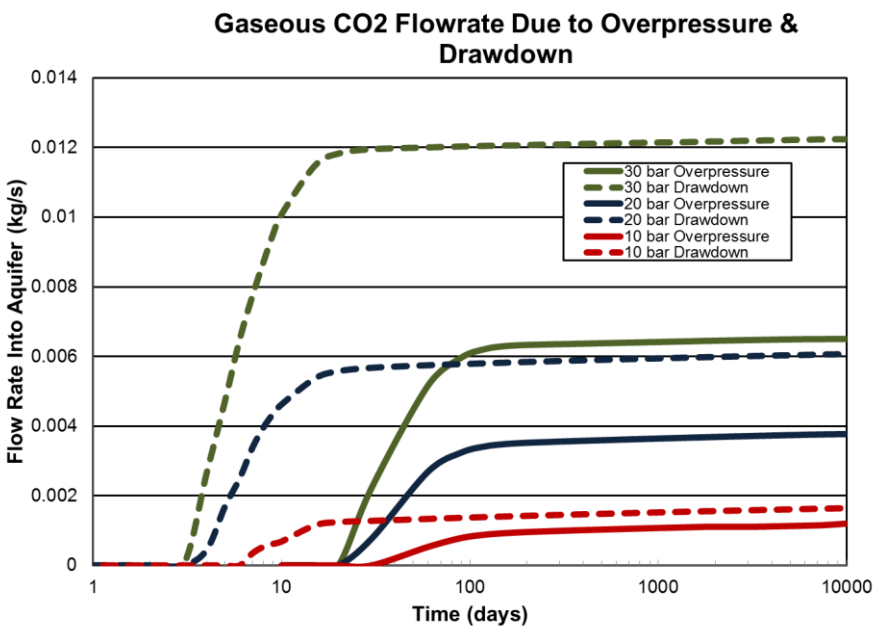

Figure 14: Exsolved gaseous CO_2 flow rate into the DWA at various overpressures and drawdowns.

3.8 Leakage Plume Behavior Post Injection

Once overpressure or drawdown has been established such that CO_2 laden brine is flowing, there is a concern that as CO_2 exsolves that it might generate a self-enhancing system whereby exsolution causes a solution gas drive that persists beyond the overpressure or drawdown event. In order to examine these effects as well as leakage plume behavior, the model from section 3.2 is set up with an 8-inch diameter well with a permeability of $1x10^{-8}$ $m^{2.}$ The storage formation is overpressured by 20 bar and the simulation is run for 100 years.

The dissolved CO_2 leakage plume in the DWA extends out 315 m after 100 years of leakage. In addition, gaseous CO_2 has developed and accumulated along the top of the DWA with a radial extent of 300 m. At the end of the 100-year injection, the outer radial ring pressure is returned to hydrostatic conditions. Within 60 days, the reduction in overpressure reaches the wellbore. As soon as this occurs, the upward flow of CO_2 laden brine ceases.

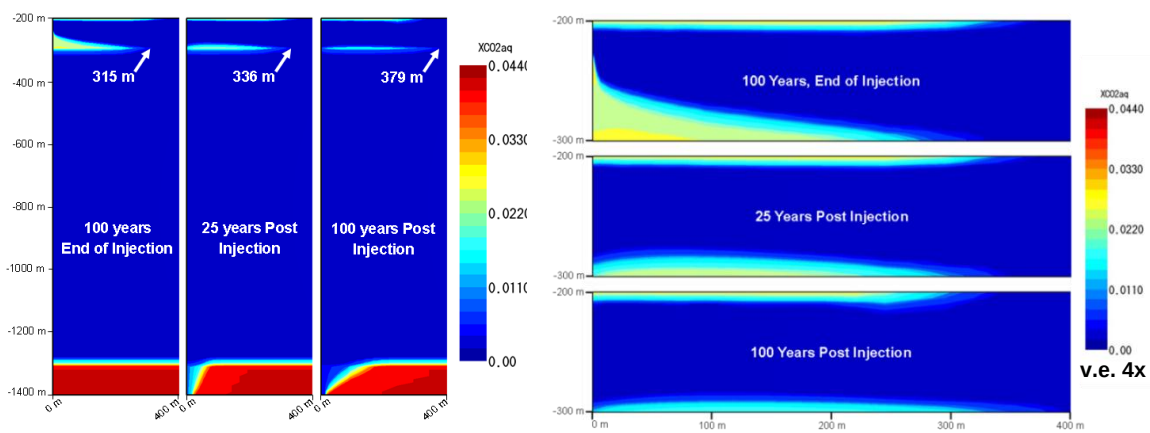

Figure 15: Dissolved CO_2 plume migration in the entire system and in the DWA after 100 years of leakage due to overpressure.

No solution gas drive effects are observed in the simulated system. Because the dissolved CO_2 in the storage formation is only a small fraction of the total fluid mass (4.4%), with less than 20% of that coming out of solution in the wellbore and DWA, the overall flow rate is dominated by the brine and not controlled by exsolving CO_2. Therefore, for the simulated scenario, in the absence of an external pressure disturbance, the exsolving CO_2 is unable to establish a solution gas drive.

Once overpressure ceases, water and CO_2 in the DWA begin flow back down the wellbore and eventually reach a steady downward flow rate of 0.19 kg/s (~3 gal/min) for the water. Due to CO_2 flowing back down the wellbore, after 25 years 7% of the total leaked CO_2 has been flushed down the wellbore while 15.8% has been at 100 years. However, the gaseous plume is diminished much faster than the dissolved CO_2 plume. After 25 years, 29% has left the DWA while 54.5% is removed after 100 years.

Initially, the leaked CO_2 laden brine flows down the well due to its density and the lack of a continued pressure head for induce upward flow. However, once this initial effect ceases, the fluid around the wellbore in the DWA remains denser than the fluid below it, allowing for downward migration. As water in the DWA contacts the gaseous CO_2 plume, the CO_2 is stripped into the dissolved phase in the water, increasing its density. This fluid then drains down the wellbore, allowing more unsaturated water to contact the gaseous plume. Therefore, the bottom of the gaseous CO_2 plume along the top of the aquifer is constantly being contacted by unsaturated water moving past it. The reduction in the gaseous and dissolved CO_2 plume in the DWA is shown in figure 15.

In addition to reducing the plume in the DWA, the area around the wellbore in the dissolved CO_2 storage formation is being diluted in respect to CO_2 content (figure 15). This is due to the downward migration of water from the DWA. For this simulated case, the downward migration of fluid post injection further reduces the leakage risks posed by dissolved CO_2.

3.9 Comparing Supercritical CO_2 Leakage to CO_2 Dissolved Brine Leakage

Leakage of dissolve CO_2 in brine may be less severe than if supercritical or gaseous CO_2 encounters an improperly abandoned wellbore for several reasons. Chiefly, the higher density of brines with dissolved CO_2 restricts upward movement without some degree of overpressure or overlying drawdown. On the other hand, highly buoyant supercritical or gaseous CO_2 is capable of moving upward through leakage pathways without any secondary pressure drive. Secondly, because dissolved phase CO_2 only constitutes a small fraction of the total fluid mass in a brine, compared to supercritical or gaseous CO_2, there is less total CO_2 available for leakage. Thirdly, the viscosity of CO_2 laden brine is much higher than supercritical or gaseous CO_2.

To compare the magnitude of the leakage and the plume extent in the DWA due to leakage of dissolved and supercritical CO_2, the scenario from section 3.2 is used to model both scenarios. In order to compare equal masses of CO_2 for both the dissolved and supercritical leakage simulations, the CO_2 in the storage formation had to be modified in order for a gas phase to be present. For the dissolved model, the mass of CO_2 in the storage formation is distributed throughout the entire 100-meter thick formation as a dissolved phase. To allow for an equal mass comparison, the same mass of CO_2 is placed

into only the upper 20 m of the storage formation. Because the same mass of CO_2 is placed into a smaller volume, the CO_2 is above the solubility of the brine around it, allowing for a supercritical phase saturation of 35.2% in the storage formation.

An 8-inch diameter $1x10^{-8}$ m^2 permeability well is used for both simulations. In order to compare to dissolved leakage, which requires a pressure differential for leakage, a moderate overpressure of 10 bar is induced. Without this overpressure, no leakage of dissolved CO_2 will occur. In addition to the 10 bar of overpressure case, the supercritical case is also simulated without any formation overpressure to show the supercritical leakage plume due only to buoyancy.

While both simulations have a temperature gradient, they are simulated isothermally due to limitations of the ECO2N simulator. While a new version is in development, ECO2N cannot currently model the CO_2 phase change between gas and liquid. However, as supercritical CO_2 expands due to depressurization during wellbore leakage, Joules-Thompson cooling effects occur which significantly lower the temperature in the wellbore (Pruess, 2008). This drop in temperature can causes a phase change from gaseous to liquid CO_2 within the wellbore. While interesting flow effects may result from this phase change, it is not the focus of this study. The use of an isothermal condition affects the leakage plume for both simulations, but it still is a useful comparison.

Because equal masses of CO_2 are used in the storage formation, an equal degree of leakage for both the dissolved and supercritical CO_2 scenarios would represent equal risks. However, the supercritical leakage simulation allowed for almost 14x more CO_2 to

be leaked compared to the dissolved case after 50 years. In addition, the maximum plume extent in the DWA is 4.6x larger for the supercritical leakage simulation.

In both simulations, both gaseous and dissolved plumes exist. In the CO_2 laden brine simulation, the dissolved plume in the DWA comes directly from the leaked dissolved CO_2. However, the dissolved plume for the case of supercritical leakage is due to CO_2 being stripped away and dissolved into resident brine as it migrates upward. Although changing multiphase flow parameters and density effects could reduce the extent of the gaseous plume, it is expected that a gaseous leakage plume will likely be much larger than a CO_2 laden brine plume for a given storage formation overpressure due to its buoyancy. For both simulations, the CO_2 plumes (gaseous and dissolved) after 50 years can be seen in figures 16 and 17.

For the additional simulation of supercritical leakage due only to buoyancy, more supercritical CO_2 escapes through the wellbore compared to dissolved leakage under 10 bar overpressure. After 50 years, the mass of CO_2 leaked due only to buoyancy is over 12x larger than the dissolved leakage simulation.

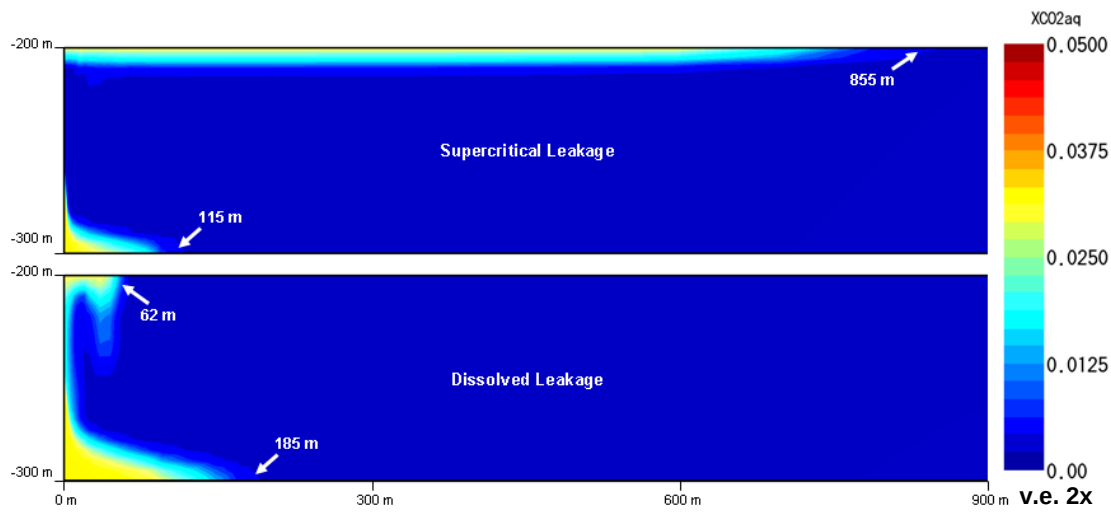

Figure 16: Dissolved CO_2 plumes in the DWA at 50 years for both supercritical and CO_2 laden brine leakage models.

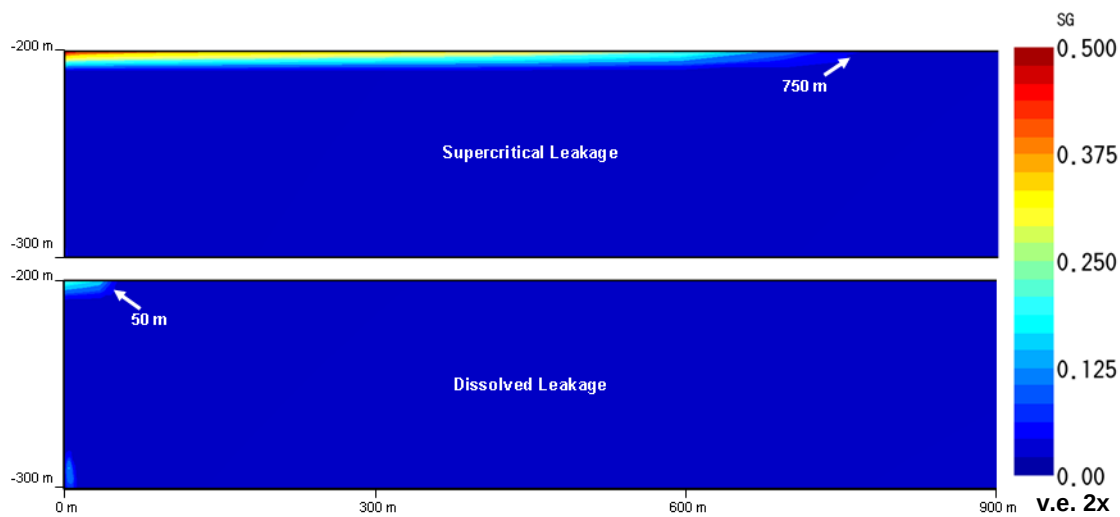

Figure 17: Gaseous CO_2 plumes in the DWA at 50 years for both supercritical and CO_2 laden brine leakage models.

4. SIMPLE STRATIFIED MODEL

In order to move beyond the base case, the region containing the impermeable layer is modified so that effects due to interbedded stratigraphy can be examined. This allows for

a more complex analysis of how a CO_2 laden brine leakage scenario will behave given a more realistic geologic system.

A new material with the same properties as the DWA is created and assigned to four 100 m thick zones along the length of the model with top elevations of 350, 550, 750, and 950 m below the ground surface respectively. All formations are penetrated by an 8-inch diameter $1x10^{-8}$ m^2 permeability well. Simulation results are compared to unstratified models in order to recognize trends between the leakage plumes simulated in both scenarios.

4.1 Overpressure

The stratified model is run for fifty years with an overpressure of 20 bar. After 50 years, no CO_2, dissolved or gaseous, has reached the drinking water aquifer. The four interbedded aquifers provide significant leakage pore space for the CO_2 laden brine as it moves up the wellbore. Because the majority of the CO_2 is dissolved in the leaking brine, the effects of capillary entry pressure and relative permeability are minimal. Therefore, the majority of the dissolved CO_2 is transported into interbedded layers as a part of the single aqueous phase brine. Furthermore, the largest amount of leaked brine migrates directly into the closest overlying formation. Some gaseous CO_2 leaks into the stratified layers as well. CO_2 exsolution occurs within the wellbore during upward migration. However, instead of continuing to migrate upward, the gaseous CO_2 enters into the interbedded stratigraphy. Both the dissolved and gaseous CO_2 plumes in the stratified system can be seen in figure 18.

In the system modeled, the presence of interbedded stratigraphy reduces the leakage risk for CO_2 into a DWA. Further simulations are run with overpressures as high as 50 bar. Even at this high overpressure, the CO_2 never moves into the drinking water aquifer, but instead has a greater degree of accumulation in the interbedded aquifers between the storage formation and the DWA.

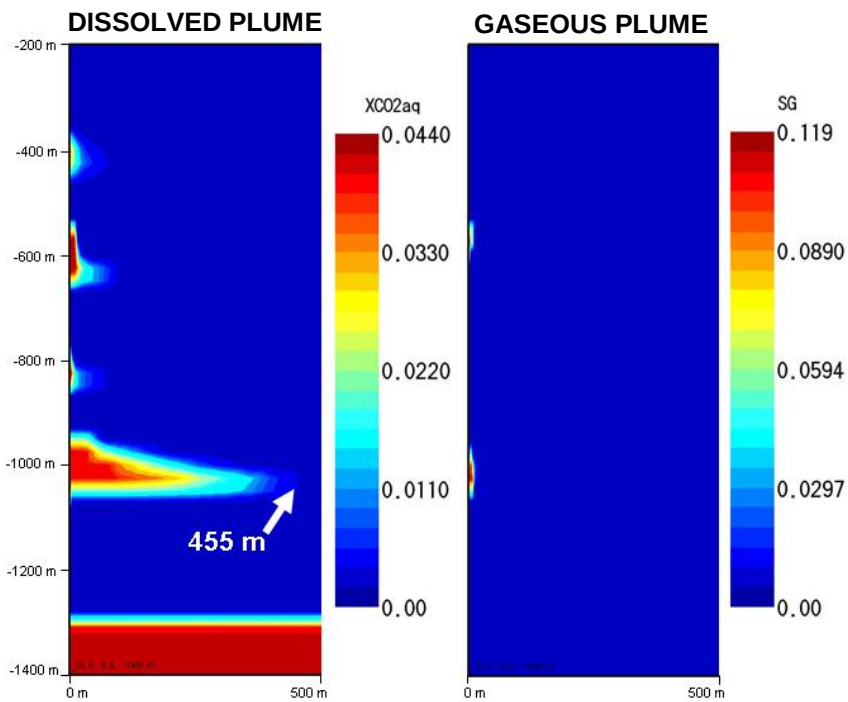

Figure 18: Dissolved and gaseous leakage plumes at 50 years for the stratified simulation at 50 years of leakage.

Because a small amount of gas development occurs, additional simulations are performed in order to observe the effects of different gas entry pressures on leakage plume development in the system. Whenever gas exsolves in overlying stratigraphy, it has the potential to block the pore space, reducing aqueous phase effective permeability,

and impeding further entry of brine containing dissolved CO_2. Therefore, models are run with an entry pressures an order of magnitude above and below the original stratified model.

Lowering the gas entry pressure allows a higher amount of gas to move more easily into interbedded aquifers above the storage formation. Therefore, less pore space is blocked by gas along the wellbore/permeable formation contact. This allows more brine to flow into the interbedded permeable layers, reducing upward migration. Conversely, raising the entry pressure impedes lateral flow of gas, blocking pore space and causing more CO_2 laden brine to migrate further up the wellbore. However, since gas phase development is not a major factor in this system, the CO_2 laden brine only moves slightly further up the wellbore and never reaches the DWA.

In the afore mentioned simulations, no salinity gradient is used between the upper DWA and the storage formation so that the entire model is fresh water except for the CO_2 storage formation. Because the brine in the storage formation has a low salinity, the addition of a salinity gradient has little effect. However, an additional simulation is performed where a linear salinity gradient is used ranging from fresh water in the DWA to 150,000 mg/l in the storage formation. Because the higher salinity causes the brine to be denser, a higher degree of overpressure is necessary to drive the brine upward. In this stratified model, the higher salinity results in all of the CO_2 laden brine leaking directly into the interbedded aquifer above the storage formation as can be seen in figure 19. No further upward migration occurs.

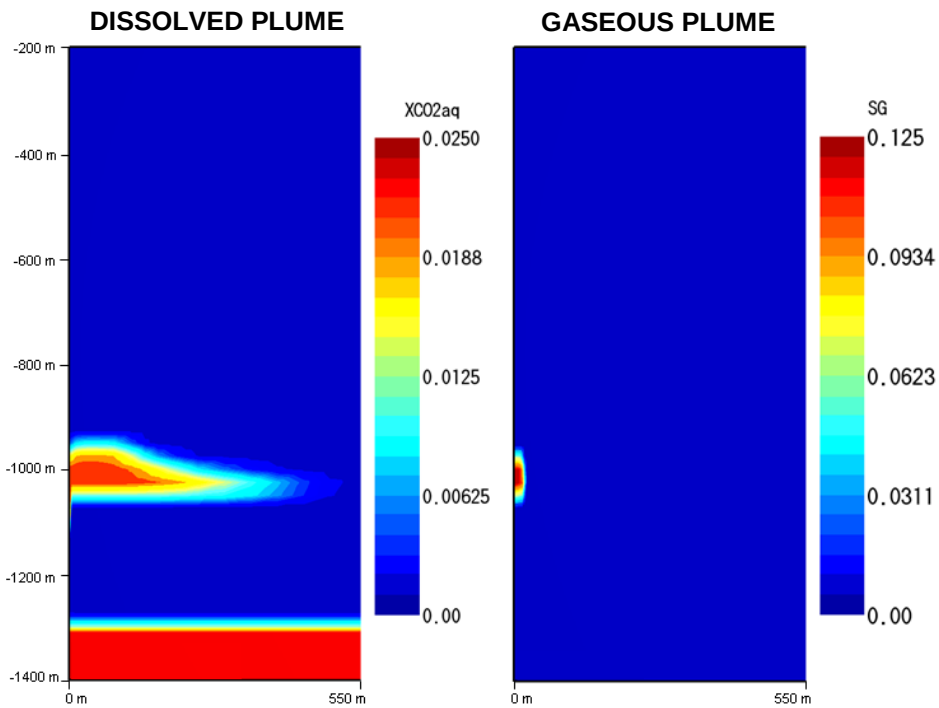

Figure 19: Dissolved and gaseous leakage plumes at 50 years for the 150,000 mg/l salinity stratified simulation at 50 years of leakage.

4.2 Effects of DWA Drawdown

The stratified model is again used to simulate leakage effects due to DWA drawdown when permeable stratified layers are present. In order to examine a worst-case scenario, the wellbore is made highly permeable ($1x10^{-5}$ m^2) to maximize the possible amount of upward flow due to drawdown. The DWA is then drawn down 20 bar (~200 m head).

The horizontal flow rate in each formation along the entire length of the wellbore at 50 years can be seen in in figure 20. As fluid is flowing into the upper aquifer, it is being pulled directly from the interbedded aquifers below. In this scenario, only a small amount of CO_2 laden brine is drawn out of the storage formation but it is never pulled up the well far enough to enter overlying permeable layers. The vertical flow rate in the

wellbore during drawdown can be seen in figure 21. Again, the upward flow of fluid from each formation is reduced with depth as each successive permeable layer below the DWA contributes less to the overall flow rate.

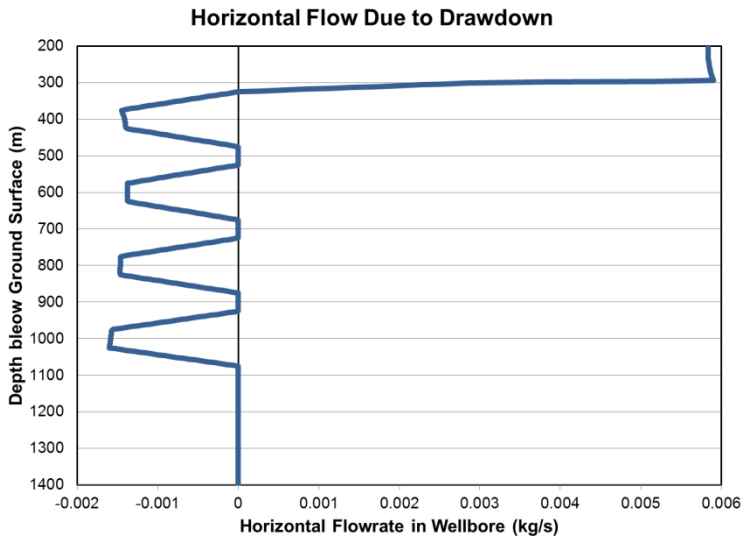

Figure 20: Horizontal brine flow rate along the wellbore due to DWA drawdown at 50 years in the stratified simulation

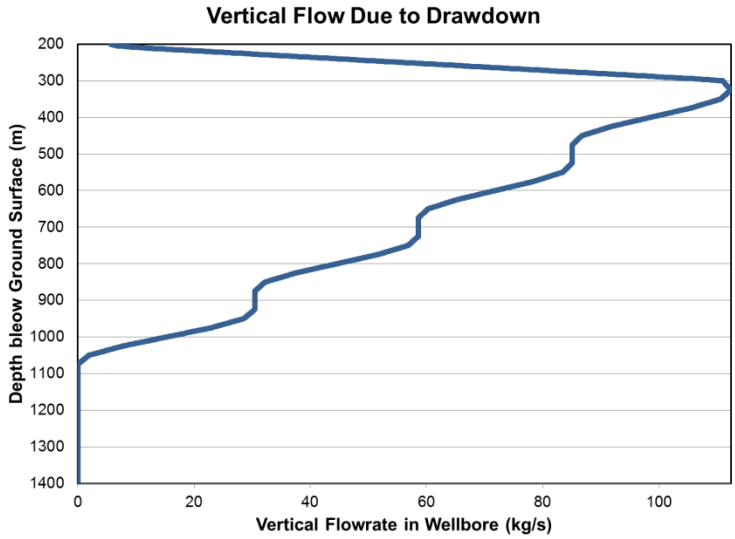

Figure 21: Vertical brine flow rate along the wellbore due to DWA drawdown at 50 years in the stratified simulation.

Whenever interbedded permeable layers exist between a formation being drawn down and a dissolved CO_2 storage formation, the possibility of dissolved CO_2 leakage is greatly reduced by the presence of the interbedded permeable layers.

4.3 Dissolved CO_2 Injection into Interbedded Formations Connected by an Open Well

All previous simulations are based upon storage of dissolved CO_2 in the bottom formation of the system being modeled. In order to examine any potential adverse effects due to the shallow dissolved CO_2 injection where stratified layers exist both above and below the injection zone, the simple stratified model is modified such that no CO_2 is initially present in the bottom formation. Instead, the 100 m thick interbedded formation with a top depth 750 m below ground surface is used as the dissolved CO_2 storage formation. This allows for the possibility of CO_2 laden brine interactions with three permeable formations above and two below while still being below the supercritical depth for CO_2 where solubility is higher. A linear salinity gradient of 0 to 260,000 mg/l is incorporated over the length of the model. The CO_2 is dissolved into the brine at its maximum solubility (2.5%) for the formation's initial P/T/S conditions. Similar to other simulations, an 8-inch diameter $1x10^{-8}$ m^2 permeability well penetrates all formations.

After overpressurizing the interbedded storage formation by 20 bar for 50 years, the majority of the leaked CO_2 has moved symmetrically into the permeable layers below and above the injection zone. Furthermore, the leakage plumes above and below the overpressurized formation have an interesting shape. Because the leaked brine is less

saline than the waters below, upon entry into the formation, it is slightly more buoyant than the surrounding waters, causing gravity override. Similarly, the leaked fluid is denser than the fluid in overlying formations, again causing gravity override of the resident fluid. Although most of the leaked CO_2 leaks directly into formations above and below, some CO_2 both dissolved and gaseous migrates further upward and eventually into the DWA.

The presence of a larger exsolved gas phase above the storage formation than in previous simulations is due to the storage formation occurring at a shallower depth. Because the critical point depth for CO_2 is quickly encountered during upward migration, larger amounts of gas exsolve. Both the dissolved and gaseous leakage plumes can be seen in figure 22.

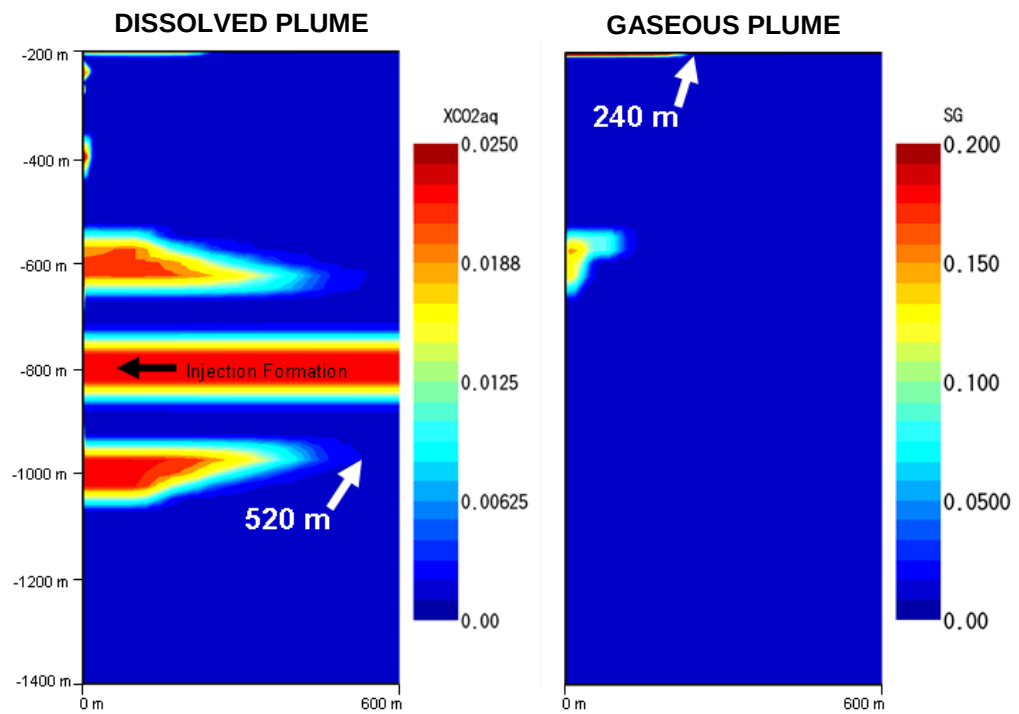

Figure 22: Dissolved and gaseous CO_2 plumes due to leakage from a stratified layer at 50 years.

5. WABAMUN LAKE STRATIFIED MODEL

In order to examine how dissolved CO_2 laden brine may be expected to leak in a real geologic system, a detailed stratified model based on data from the Wabamun Project website is used (AGS, 2011). The project website is a repository for rock core data as well as descriptions of the pressure, temperature, and stratigraphy of the site.

Data available through the project website as well as research conducted by (Bennion and Bachu, 2005; Bennion and Bachu, 2006a; Bachu and Bennion, 2008a; Bennion and Bachu, 2008b)was compiled to create three geologic materials: aquifer, weak aquitard, and a strong aquitard which correlate to the available materials from the available stratigraphic model (see appendix A). Based on the stratigraphic model, 37 stratified layers are created as shown in figure 23.

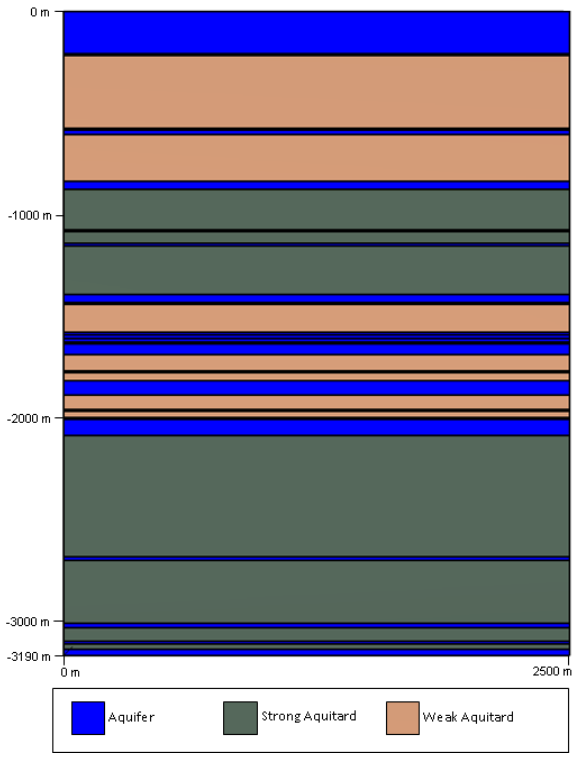

Figure 23: Model setup for Wabamun Lake stratified model showing the three rock types used and the 37 model layers.

The model has a radial dimension of 2,500 m and a total depth of 3,190 m starting from the ground surface. As in previous models, an 8-inch (0.2 m) diameter $1x10^{-8}$ m^2 permeability well in the central radial grid block penetrates all formations. A uniform vertical grid spacing of 5 m is used while a total of 62 radial grid block are used ranging from the 0.1 m well block to 100 m at the radial boundary.

Bennion and Bachu (2005) reports an average geothermal gradient of 25°C/km for the Wabamun Lake area, therefore this value is used over the length of the entire model, assuming a surface temperature of 4°C. Three pressure zones are created in the model according to information given on the website. From 0-880 m, a hydrostatic pressure

gradient is used. The lower formations below this depth are underpressurized and are given a linear pressure gradient with a pressure of 5.2×10^6 Pa at 880 m and 3×10^7 Pa at 3190 m. In addition, the Cardium sandstone, which is a 10-meter thick hydrocarbon-bearing zone at a bottom depth of 1160 m, is overpressurized with a pressure of 2×10^7 Pa.

Table 8: Rock Properties for Wabamun Lake Stratified Model

Property	Value	Comment
Entire Model		
Thermal Conductivity (W/m·°C)	2.51	Representative of values used in similar studies (Pruess, 2008)
Heat Capacity (J/Kg·°C)	920	
Rock Density (Kg/m^3)	2600	
Salinity (mg/l)	0-10,000 mg/l from 0-880 m depth 20,000-248,000 mg/l from 880-3190 m depth	From Wabamun Project website
Aquifer		
Permeability (m^2)	1×10^{-14}	Average of all aquifer rock type data
Porosity	0.16	
Weak Aquitard		
Permeability (m^2)	1×10^{-16}	Average of all weak aquitard rock type data
Porosity	0.08	
Strong Aquitard		
Permeability (m^2)	1×10^{-20}	Average of all strong aquitard rock type data
Porosity	0.062	
Wellbore		
Permeability, (m^2)	1×10^{-8}	
Porosity	0.98	
Well Diameter (m)	0.2 (8 inch)	

Similar to the base case, the outermost ring is maintained as a fixed state condition (constant pressure, temperature, salt concentration, CO_2 saturation) along the entire

vertical length of the model. Pressure in the outer ring can be increased to over pressurize the desired storage formation.

The relative permeability and capillary pressure parameters used in the model are found in table 9. For simplification, the Corey's relative permeability equation (Corey, 1954)is used for all materials within the model:

$$k_{rl} = \left(\frac{S_l - S_{lr}}{1 - S_{lr} - S_{gr}} \right)^4 \qquad \textbf{Eq. 24}$$

$$k_{rg} = \left(1 - \left[\frac{S_l - S_{lr}}{1 - S_{lr} - S_{gr}} \right] \right)^2 \bullet \left(1 - \left[\frac{S_l - S_{lr}}{1 - S_{lr} - S_{gr}} \right]^2 \right) \qquad \textbf{Eq. 25}$$

Capillary pressure was again calculated using the van Genuchten model. Values for P_0, describing the capillary entry pressure, are derived by taking the entry pressures calculated in (Bachu and Bennion, 2008a; Bennion and Bachu, 2008b) and assigning an average value for each of the three material groups: aquifer, weak aquitard, and strong aquitard.

Table 9: Relative Permeability and Capillary Pressure Parameters for Wabamun Lake Stratified Model

Relative Permeability Corey's Model	**S_{lr}**	**S_{gr}**		
All Rock Units	0.1	0.2		
Wellbore	0.01	0.01		
Capillary Pressure Van Genuchten Model	**λ**	**S_{lr}**	**P_0 (kPa)**	**S_{ls}**
Aquifer	0.457	0.3	10.4	1
Weak Aquitard	0.457	0.3	57.1	1
Strong Aquitard	0.457	0.3	344.8	1
Wellbore	Zero Capillary Pressure			

Simulations of dissolved CO_2 leakage in open wells are performed using the Wabamun Lake model in order to evaluate the type of leakage plume that may be expected in a realistic geologic system. Dissolved CO_2 is first allowed to leak out of the Basal Cambrian formation at the bottom of the model due to overpressure. Then, a simulation is run where dissolved CO_2 is injected into the 70 m thick Wabamun formation at a bottom depth of 1900 m below the ground surface.

5.1 Leakage from Basal Cambrian Formation

In order to evaluate a high dissolved leakage, the Basal Cambrian storage formation is overpressurized 30 bar which is near the maximum overpressure expected due to injection in Zhou et al., 2010. In addition, a moderate well permeability of $1x10^{-8}$ m^2 is used.

In Figure 24, which begins at a top depth of 1800 m below the ground surface, the leakage plumes after 50 years of overpressure can be seen. A significant amount of dissolved CO_2 has leaked into the five aquifers overlying the Basal Cambrian formation; however, no fluid has migrated above the permeable Wabamun formation. All of the CO_2 accepting aquifers lie in the underpressurized zone; therefore, they are capable of accepting a great deal of leaked fluid. For further evaluation, another simulation is run with an overpressure of 50 bar. No further upward migration occurs, however larger plumes develop in the first five overlying aquifers. The uppermost small leakage plume is slightly buoyant due to being warmer than the resident brine. In addition, a small gas

plume develops in the permeable Cathedral formation directly above the Basal Cambrian, however, no other gas phase exsolves.

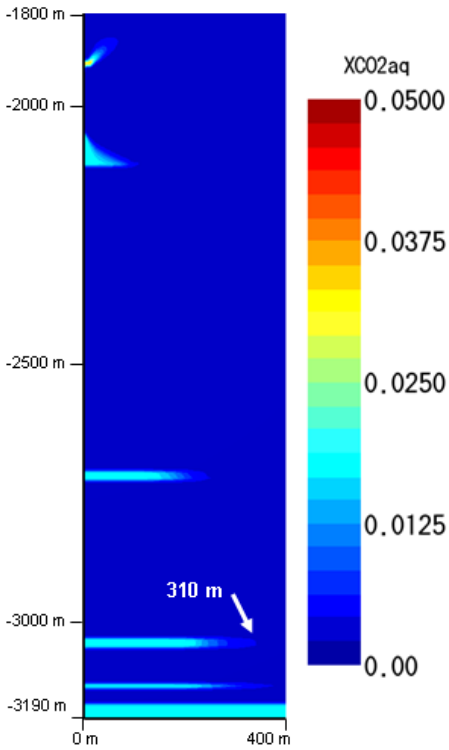

Figure 24: Dissolved leakage plume due to injection into the Basal Cambrian formation at 50 years (note that the top depth is only -1800 m).

5.2 Leakage from Wabamun Lake Formation

In order to evaluate leakage effects due to injection in an interbedded layer, CO2 is dissolved into the permeable Wabamun formation at it maximum solubility (3.1%). The formation is then overpressurized 30 bar to induce flow into the open wellbore. Similar to the simple stratified model of section 4.3, the dissolved CO_2 laden brine flows into permeable formations above and below the injection zone because the lower portion of the model is underpressurized initially, this allows for greater downward migration of

leaked fluid. Therefore, dissolved CO_2 migrates into all of the permeable formations below the injection zone. However, the largest plumes occur directly above and below the injection zone. While upward migration of CO_2 laden brine does occur, it never moves up further than the permeable Ellerslie formation at 1620 m below the ground surface (figure 25).

Even though upward leakage is not significant, because CO_2 does migrate into these secondary formations, all permeable layers must be considered during site selection for a CO_2 injection project. Due to possible secondary leakage into permeable formations, wells that penetrate any within the storage site's area of review will likely need to be investigated for its leakage potential and monitored throughout the life of the project.

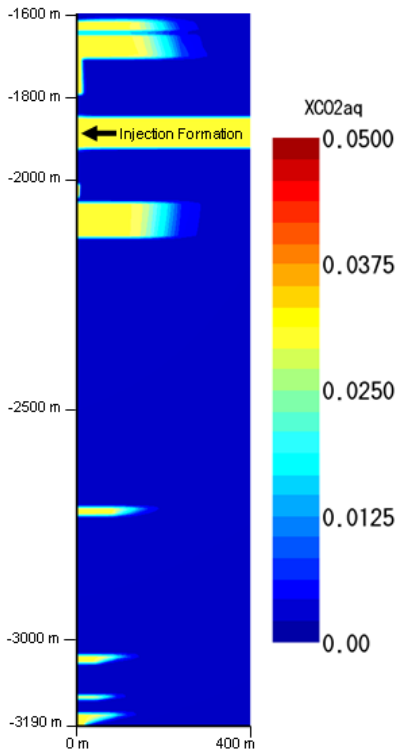

Figure 25: Dissolved leakage plume due to dissolved CO_2 leakage from the Wabamun formation at 50 years (note that the top depth is only -1600 m).

6. SUMMARY

Simulations have been performed to evaluate risks posed to leakage of CO_2 laden brine through poorly sealed or improperly abandoned wellbores. In addition, an analytical model has been proposed that predicts order of magnitude leakage behavior of brine through wells. Although it only describes flow of uniform density fluid, the analytical model is useful at describing how system parameters control leakage magnitudes.

Through analytical and numerical models, it has been found that the overriding controls of wellbore leakage of dissolved brines are storage formation overpressure, well permeability, and well diameter.

In most leakage scenarios where the wellbore is not an open pipe but instead is blocked in some fashion, the permeability of the well controls the leakage rate of CO_2 laden brine into permeable formations. However, if the endpoint case of leakage through a completely open well were to occur, the permeabilities of the geologic formations will provide more resistance to fluid flow. As a result, there is probable upper limit to the leakage flow of brine, even with an open well.

For the endpoint case where no layers are present between the storage formation and the DWA, significant amounts of gas can exsolve during leakage to form a separate gas phase. However, in a more realistic case where interbedded permeable layers are present, simulation results show that while gas phase exsolution does occur, large gaseous plumes are not observed.

In the simulations performed, CO_2 laden brine leakage due to drawdown of overlying drinking water aquifers poses minimal risks if stratified permeable layers are present. During drawdown, fluid is preferentially drawn out of formations directly underneath the formation being pumped. Therefore, in a typical stratified system, it is possible that a deep CO_2 storage formation will not be affected by drawdown.

After overpressure has ceased, leakage of CO_2 laden brine does not continue. No solution gas drive effects are observed in the simulations. Furthermore, after injection has ceased, significant amounts of the leaked CO_2, especially the gaseous plume, may be flushed back down the wellbore due to a depth decreasing density gradient in the system. This serves as a natural mechanism for CO_2 leakage mitigation.

The numerical simulations are unable to capture the exact behavior of dissolved CO_2 leakage for an open wellbore. Although effects due to turbulent friction as well as multiphase flow regimes are not considered, the high permeability model results still provide valuable insights into the behavior of dissolved CO_2 leakage.

During overpressure, dissolved leakage plumes can develop both above and below the storage site where CO_2 is being injected. Although these secondary plumes remain at depths that are considered secure, they must be considered as possible secondary leakage sources. Therefore, when performing site selections, it will be imperative to examine wells at all depth and not just wells that penetrate the target formation in the area of review boundary.

APPENDIX A

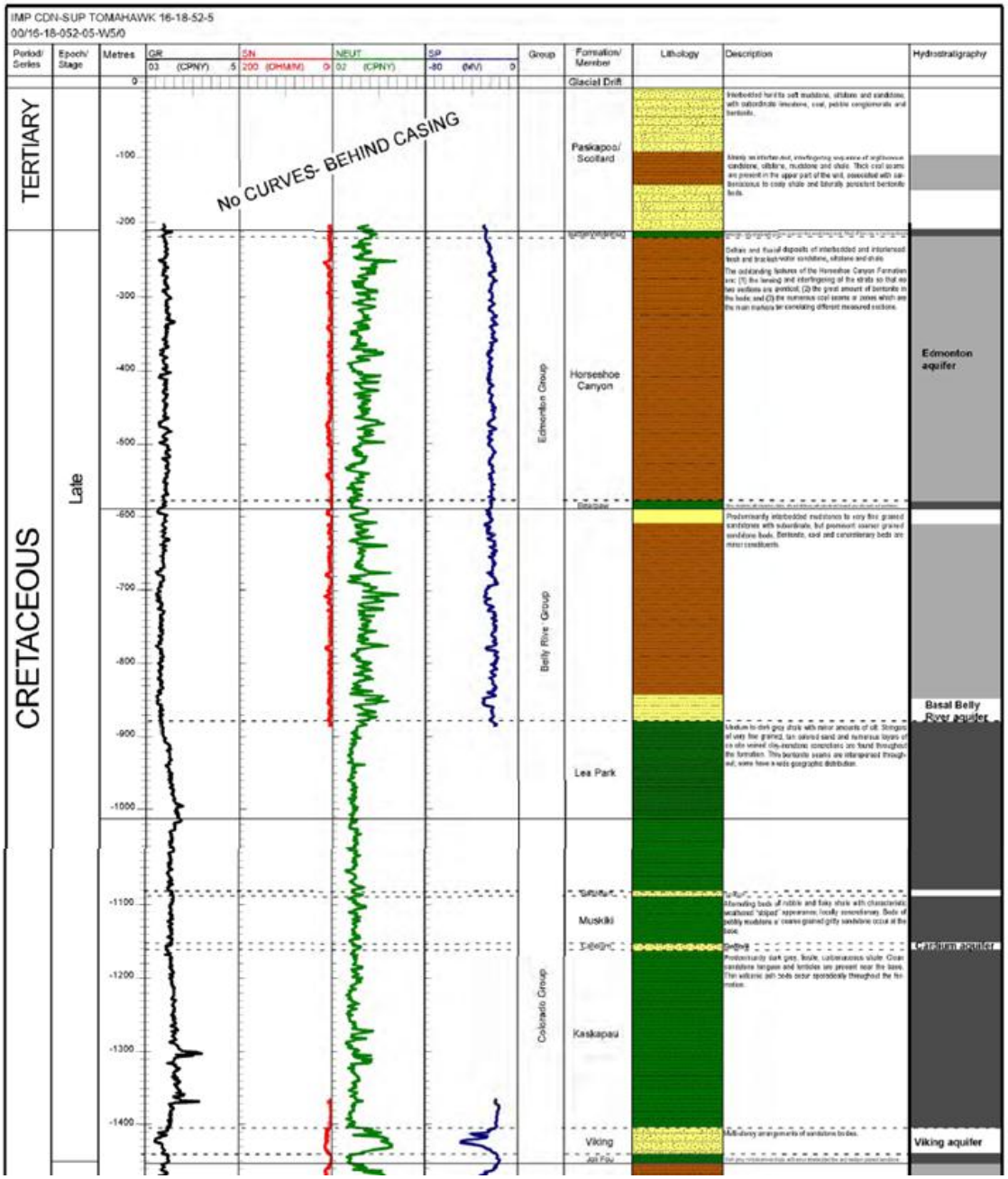
IMP CDN-SUP TOMAHAWK 16-18-52-5
00/16-18-052-05-W5/0
Period/ Series
Epoch/ Stage
Metres
GR
SN
NEUT
SP
Group
Formation/ Member
Lithology
Description
Hydrostratigraphy
TERTIARY
CRETACEOUS
Late
No CURVES- BEHIND CASING
Glacial Drift
Paskapoo/ Scollard
Horseshoe Canyon
Edmonton Group
Edmonton aquifer
Belly River Group
Basal Belly River aquifer
Lea Park
Colorado Group
Muskiki
Kaskapau
Viking
Viking aquifer

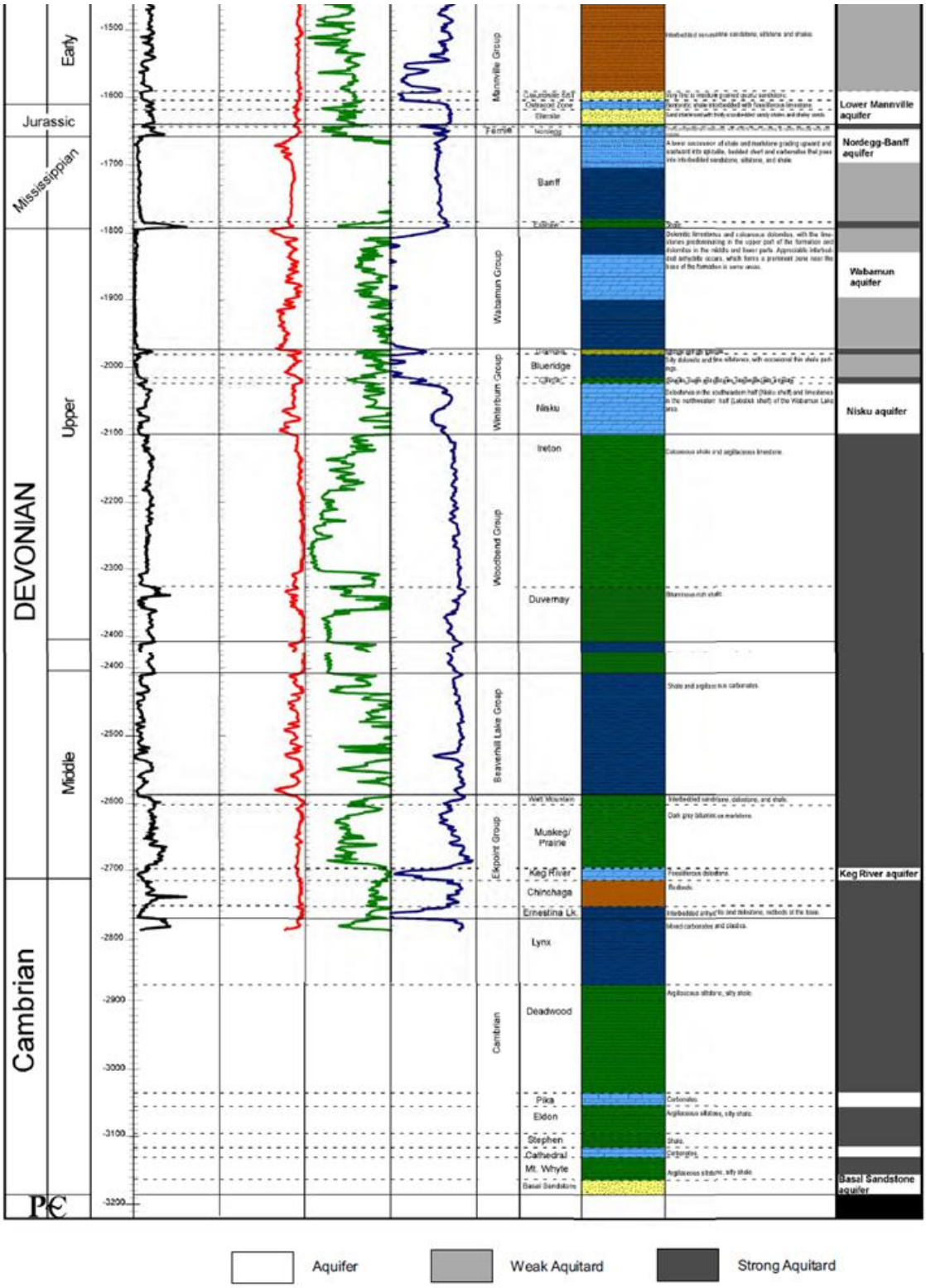
DEVONIAN
Cambrian
Early
Jurassic
Mississippian
Upper
Middle
-1500
-1600
-1700
-1800
-1900
-2000
-2100
-2200
-2300
-2400
-2500
-2600
-2700
-2800
-2900
-3000
-3100
-3200
Mannville Group
Fernie
Wabamun Group
Winterburn Group
Woodbend Group
Beaverhill Lake Group
Elkpoint Group
Cambrian
Nordegg
Banff
Blueridge
Nisku
Ireton
Duvernay
Muskeg/
Prairie
Keg River
Chinchaga
Ernestina Lk.
Lynx
Deadwood
Pika
Eldon
Stephen
Cathedral
Mt. Whyte
Lower Mannville aquifer
Nordegg-Banff aquifer
Wabamun aquifer
Nisku aquifer
Keg River aquifer
Basal Sandstone aquifer
Aquifer
Weak Aquitard
Strong Aquitard

7. REFERENCES

AGS, 2011, Test Case for Comparative Modelling of CO2 Injection, Migration and Possible Leakage - Wabamun Lake Area, Alberta, Canada, <http://www.ags.gov.ab.ca/co2_h2s/wabamun/Wabamun_base.html> Accessed 2/1, 2011.

Bachu, S. and J. J. Adams, 2003, Sequestration of CO2 in geological media in response to climate change: capacity of deep saline aquifers to sequester CO2 in solution, Energy Conversion and Management, vol. 44, no. 20, p. 3151-3175.

Bachu, S. and B. Bennion, 2008a, Effects of in-situ conditions on relative permeability characteristics of CO 2-brine systems, Environmental Geology, vol. 54, no. 8, p. 1707-1722.

Bennion, B., Bachu, S., Relative Permeability Characteristics for Supercritical CO2 Displacing Water in a Variety of Potential Sequestration Zones in the Western Canada Sedimentary Basin. Paper SPE 95547, presented at the 2005 SPE Annual Technical Conference and Exhibition, Dallas, TX, USA, October 9-12, 2005.

Bennion, B. and S. Bachu, 2008b, Drainage and imbibition relative permeability relationships for supercritical CO2/brine and H2S/brine systems in intergranular sandstone, carbonate, shale, and anhydrite rocks, SPE Reservoir Evaluation & Engineering, vol. 11, no. 3, p. 487-496.

Bennion B. and S. Bachu, 2006a, The Impact of Interfacial Tension and Pore-size Distribution/Capillary Pressure Character on CO2 Relative Permeability at Reservoir Conditions in CO2–brine Systems. Paper presented in SPE/DOE symposium on improved oil recovery, Tulsa, Oklahoma, USA, 22–26 April, 2006.

Benson, S. M., Cook, P., Coordinating Lead Authors, J. Anderson, S. Bachu, H. B. Nimir, B. Basu, J. Bradshaw, G. Deguchi, J. Gale, G. von Goerne et al, 2005, Underground geological storage, in IPCC Special report on Carbon Dioxide Capture and Storage, Chapter 5, Cambridge, U.K., Cambridge University Press.

Birkholzer, J. T., J. P. Nicot, C. M. Oldenburg, Q. Zhou, S. Kraemer, and K. Bandilla, 2011, Brine flow up a well caused by pressure perturbation from geologic carbon sequestration: Static and dynamic evaluations, International journal of greenhouse gas control.

Burton, M. M. and S. Bryant, 2007, Eliminating Buoyant Migration of Sequestered CO2 through Surface Dissolution: Implementation Costs and Technical Challenges, SPE 110650, Proceedings, 2007 SPE Ann. Tech. Conf. Exhib., Anaheim, CA, 11-14 November, 2007.

Burton, M. M. and S. L. Bryant, 2009, Surface dissolution: Minimizing groundwater impact and leakage risk simultaneously, Energy Procedia, vol. 1, no. 1, p. 3707-3714.

Celia, M. A., S. Bachu, J. M. Nordbotten, S. E. Gasda, and H. K. Dahle, 2004, Quantitative estimation of CO2 leakage from geological storage: Analytical models, numerical models and data needs, Proceedings of the 7th International Conference on Greenhouse Gas Control Technologies (GHGT-7), September 5-9, 2004, Vancouver, Canada, v.I, 663-672.

Corey, A. T., 1954, The interrelation between gas and oil relative permeabilities, Producers Monthly, vol. 19, no. 1, p. 38-41.

Doughty, C., 2007, Modeling geologic storage of carbon dioxide: Comparison of non-hysteretic and hysteretic characteristic curves, Energy Conversion and Management, vol. 48, no. 6, p. 1768-1781.

Ebigbo, A., H. Class, and R. Helmig, 2007, CO 2 leakage through an abandoned well: Problem-oriented benchmarks, Computational Geosciences, vol. 11, no. 2, p. 103-115.

Enick, R. M. and S. M. Klara, 1990, CO 2 solubility in water and brine under reservoir conditions, Chemical Engineering Communications, vol. 90, no. 1, p. 23-33.

Ennis-King, J. and L. Paterson, 2003, Rate of dissolution due to convective mixing in the underground storage of carbon dioxide, Sixth International Conference on Greenhouse Gas Control Technologies, Kyoto, vol. I, Pergamon, Amsterdam, pp. 507–510.

EPA, 2011, INVENTORY OF U.S. GREENHOUSE GAS EMISSIONS AND SINKS: 1990 – 200, available at: http://www.epa.gov/climatechange/emissions/usinventoryreport.html.

Freeze, R. A. and J. A. Cherry, 1979, Groundwater.

Gasda, S. E., S. Bachu, and M. A. Celia, 2004, The potential for CO2 leakage from storage sites in geological media: analysis of well distribution in mature sedimentary basins, Environmental Geology, vol. 46, no. 6-7, p. 707–720.

Gass, T., J. Lehr, and H. Heiss Jr, 1977, Impact of abandoned wells on ground water.

Gupta, R.S., 2001, Hydrology and Hydraulic Systems. Waveland Press, Inc., Prospect Heights, Illinois, second Edition, 2001.

Ide, S. T., S. J. Friedmann, and H. J. Herzog, 2006, CO2 leakage through existing wells: current technology and regulations, 8th International Conference on Greenhouse Gas Control Technologies, Trondheim, Norway, June 19-22, 2006.

IPCC, 2005, Intergovernmental Panel on Climate Change, Special Report on Carbon Dioxide Capture and Storage.

Leonenko, Y. and D. W. Keith, 2008, Reservoir engineering to accelerate the dissolution of CO2 stored in aquifers, Environ.Sci.Technol, vol. 42, no. 8, p. 2742-2747.

McPherson, B. and B. S. Cole, 2000, Multiphase CO2 flow, transport and sequestration in the Powder River basin, Wyoming, USA, Journal of Geochemical Exploration, vol. 69, p. 65-69.

NETL, 2010, (National Energy Technology Laboratory) 2010 Carbon Sequestration Atlas of the United States and Canada – Third Edition (Atlas III).

Nicot, J. P., 2009, Pressure perturbations from geologic carbon sequestration: Area-of-review boundaries and borehole leakage driving forces, Energy procedia, vol. 1, no. 1, p. 47-54.

Nordbotten, J. M., M. A. Celia, S. Bachu, and H. K. Dahle, 2005, Semianalytical solution for CO2 leakage through an abandoned well, Environmental science & technology, vol. 39, no. 2, p. 602-611.

Nordbotten, J. M., D. Kavetski, M. A. Celia, and S. Bachu, 2009, Model for CO2 leakage including multiple geological layers and multiple leaky wells, Environ.Sci.Technol, vol. 43, no. 3, p. 743-749.

Oldenburg, C. M. and A. P. Rinaldi, 2010, Buoyancy Effects on Upward Brine Displacement Caused by CO2 Injection, Transport in Porous Media, vol. 87, no. 2, p. 525-540.

Pan, L., C. M. Oldenburg, Y. S. Wu, and K. Pruess, 2009, Wellbore flow model for carbon dioxide and brine, Energy Procedia, vol. 1, no. 1, p. 71-78.

Pruess, K., 2008, On CO 2 fluid flow and heat transfer behavior in the subsurface, following leakage from a geologic storage reservoir, Environmental Geology, vol. 54, no. 8, p. 1677-1686.

Pruess, K., 2007, ECO2N-A fluid property module for the TOUGH2 code for studies of CO_2 storage in saline aquifers, Energy conversion and management, vol. 48, no. 6.

Smith, D. K., 1976, Cementing, Society of Petroleum Engineers, AIME, SPE Monograph, no. 4, New York, New York, and Dallas, Texas, p. 136.

Swenson, D., B. Hardeman, C. Persson, and C. Thornton. 2003. Using PetraSim to create, execute, and post-process TOUGH2 models. In Proceedings of TOUGH Symposium 2003. Berkeley, California: Lawrence Berkeley National Laboratory. http://www.esd.lbl.gov/TOUGHsymposium/TOUGHsymposium03/program.html.

Thiem, G., 1906, Hydrologische methoden. [The hydrogeologic method]. Gebhardt, Leipzig, p. 56.

van Genuchten, M. T., 1980, A closed-form equation for predicting the hydraulic conductivity of unsaturated soils, Soil Sci.Soc.Am.J, vol. 44, no. 5, p. 892-898.

Zhou, Q., J. T. Birkholzer, E. Mehnert, Y. F. Lin, and K. Zhang, 2010, Modeling basin- and plume-scale processes of CO2 storage for full-scale deployment, Ground Water, vol. 48, no. 4, p. 494-514.